1521-009X/50/7/898–908$35.00
DRUG METABOLISM AND DISPOSITION

dx.doi.org/10.1124/dmd.121.000799
Drug Metab Dispos 50:898–908, July 2022

Target-Mediated Drug Disposition Affects the Pharmacokinetics of Interleukin-10 Fragment Crystallizable Fusion Proteins at Pharmacologically Active Doses[S]

Zheng Yang, Surendran Rajendran, Vanessa Spires, Brian Poirson, Murali Gururajan, Zheng Lin, Jaren Arbanas, Stanley Krystek, James Loy, Yuan Cheng, Stephen Carl, Samantha Pace, Yun Wang, John Mehl, Shihua Xu, Krishna Vasudevan, Miranda Broz, Lois Lehman-McKeeman, Paul Morin, and Robert F. Graziano

Metabolism and Pharmacokinetics, Pharmaceutical Candidate Optimization (Z.Y.), Nonclinical Disposition and Bioanalysis (S.R., S.X.), Discovery Biotherapeutics (Z.L., J.A., P.M.), Molecular Structure and Design (S.K.), Discovery Pharmaceutics and Analytical Sciences, Pharmaceutical Candidate Optimization (Y.C., S.C., S.P., Y.W., J.M.), Discovery Oncology (V.S., B.P., M.G., R.F.G.), Translational Medicine (K.V.), and Pharmaceutical Candidate Optimization (L.L.-M.), Bristol Myers Squibb, Princeton, New Jersey; Discovery Toxicology, Pharmaceutical Candidate Optimization, Bristol Myers Squibb, Cambridge, Massachusetts (J.L.); and Discovery Oncology, Bristol Myers Squibb, Redwood City, California (M.B.)

Received December 2, 2021; accepted April 25, 2022

ABSTRACT

Fragment crystallizable (Fc) fusion is commonly used for extending the half-life of biotherapeutics such as cytokines. In this work, we studied the pharmacokinetics of Fc-fused interleukin-10 (IL-10) proteins that exhibited potent antitumor activity in mouse syngeneic tumor models. At pharmacologically active doses of ≥0.1 mg/kg, both mouse Fc–mouse IL-10 and human Fc–human IL-10, constructed as the C terminus of the Fc domain fused with IL-10 via a glycine-serine polypeptide linker, exhibited nonlinear pharmacokinetics after intravenous administration to mice at the doses of 0.05, 0.5, and 5 mg/kg. With a nominal dose ratio of 1:10:100; the ratio of the area under the curve for mouse Fc–mouse IL-10 and human Fc–human IL-10 was 1:181:1830 and 1:75:633, respectively. In contrast, recombinant mouse or human IL-10 proteins exhibited linear pharmacokinetics in mice. Compartmental analysis, using the Michaelis-Menten equation with the in vitro IL-10 receptor alpha binding affinity inputted as the K_m, unified the pharmacokinetic data across the dose range. Additionally, nontarget-mediated clearance estimated for fusion proteins was ~200-fold slower than that for cytokines, causing the manifestation of target-mediated drug disposition (TMDD) in the fusion protein pharmacokinetics. The experimental data generated with a mouse IL-10 receptor alpha-blocking antibody and a human Fc–human IL-10 mutant with a reduced receptor binding affinity showed significant improvements in pharmacokinetics, supporting TMDD as the cause of nonlinearity. Target expression and its effect on pharmacokinetics must be determined when considering using Fc as a half-life extension strategy, and pharmacokinetic evaluations need to be performed at a range of doses covering pharmacological activity.

SIGNIFICANCE STATEMENT

Target-mediated drug disposition can manifest to affect the pharmacokinetics of a fragment crystallizable (Fc)-fused cytokine when the nontarget-mediated clearance of the cytokine is decreased due to neonatal Fc receptor-mediated recycling and molecular weight increases that reduce the renal clearance. The phenomenon was demonstrated with interleukin-10 Fc-fusion proteins in mice at pharmacologically active doses. Future drug designs using Fc as a half-life extension approach for cytokines need to consider target expression and its effect on pharmacokinetics at relevant doses.

Introduction

Interleukin-10 (IL-10) belongs to the IL-10–interferon cytokine family and is a multifunctional dimeric cytokine produced by many immune cells such as T cells, B cells, and natural killer (NK) cells (Moore et al., 2001; Shouval et al., 2014). IL-10 binds to the IL-10 receptor alpha with a high affinity (0.035–0.24 nM) (Moore et al., 2001; Walter, 2014). Upon the binding, it leads to the recruitment of the IL-10 receptor beta

The work was conducted as part of employment at Bristol Myers Squibb.
All authors are current or former employees of Bristol Myers Squibb and own or previously owned the company's stocks.
dx.doi.org/10.1124/dmd.121.000799.
[S] This article has supplemental material available at dmd.aspetjournals.org.

ABBREVIATIONS: AUC_{tot}, area under the drug concentration-time curve from time 0 to infinity; CD3, cluster of differentiation 3; CL_{tot}, total plasma clearance; FACS, fluorescence-activated cell sorting; Fc, fragment crystallizable; FcRn, neonatal fragment crystallizable receptor; hFc, human fragment crystallizable; hIL-10, human interleukin-10; IL-10, interleukin-10; k_a, absorption rate constant; $k_{el,nontarget\text{-}mediated}$, nontarget-mediated first-order elimination rate constant; $k_{el,target\text{-}mediated}$, target-mediated first-order elimination rate constant; K_d, equilibrium dissociation constant; $K_{m,target\text{-}mediated}$, binding affinity to target; LLOQ, lower limit of quantitation; mAb, monoclonal antibody; mFc, mouse fragment crystallizable; mIL-10, mouse interleukin-10; mPD-1, mouse programmed death-1; PK, pharmacokinetics; QC, quality control; RU, resonance units; SPR, surface plasmon resonance; STAT3, signal transducer and activator of transcription 3; $t_{1/2}$, half-life; T_{max}, time for C_{max}; TMDD, target-mediated drug disposition; V_c, volume of distribution in the central compartment; $V_{c,apparent}$, apparent volume of distribution in the central compartment after intraperitoneal administration; $V_{max,target\text{-}mediated}$, maximum elimination rate mediated by target; V_{ss}, steady-state volume of distribution.

and produces a complex signaling cascade, including the phosphorylation of signal transducer and activator of transcription 3 (STAT3). The IL-10 receptor alpha is expressed by hematopoietic cells. Although the expression of the IL-10 receptor alpha was reported to be a few hundred per cell (Moore et al., 2001, von Haehling et al., 2015), a wide expression of the receptor in many immune cells renders meaningful target concentrations in blood and tissues such as the spleen, thymus, and lymph nodes (Liu et al., 1994), which leads to the diverse effects of IL-10 that are both anti-inflammatory and immunostimulatory. Because of the proinflammatory effect of IL-10, it was explored as an immuno-oncologic agent for treating cancer. Preclinically, the IL-10 treatment in mice led to the expansion and activation of primed CD8+ T cells and NK cells, which resulted in the regression of mouse syngeneic tumors (Berman et al., 1996; Adris et al., 1999; Mumm et al., 2011; Emmerich et al., 2012). Clinically, pegilodecakin, which is a pegylated IL-10, induced CD8+ T cell–mediated immunity in cancer patients (Naing et al., 2018). Although pegylated IL-10 did not improve efficacy in the phase III trial of advanced pancreatic cancer (Hecht et al., 2021), it showed an improvement in the overall response rate (44% vs. the historical data of 20%) when combined with anti–programmed death-1 (PD-1) antibodies in the heavily pretreated renal cell carcinoma patient population, warranting the further investigation of the IL-10 treatment (Tannir, et al., 2021).

Fragment crystallizable (Fc) fusion is a commonly employed method to extend the half-life ($t_{1/2}$) of peptides, antibody fragments, cytokines, and receptor extracellular domains (Kontermann., 2016). The mechanisms of the $t_{1/2}$ extension are presumably due to the molecular weight increases that reduce the size-dependent renal filtration and the neonatal Fc receptor (FcRn)-mediated recycling. Cytokines exhibit short $t_{1/2}$ of a few hours in humans, resulting in the requirement for more frequent dosing regimens in the clinic. For example, recombinant interferon alpha-2b (Intron-A) has a $t_{1/2}$ of 2–3 hours (Intron-A package insert, Merck & Co., Inc., Whitehouse Station, NJ), and the $t_{1/2}$ of recombinant interferon alpha-2a (Roferon-A) ranges from 3.7 to 8.5 hours (Roferon-A package insert, F. Hoffmann-La Roche Ltd, Basel, Switzerland). Similarly, recombinant IL-2 (Proleukin) exhibits a terminal $t_{1/2}$ of 1.4 hours in humans (Proleukin package insert, Clinigen, Inc., Yardley, PA). Given the therapeutic potential of cytokines (Runbeck et al., 2021) and their short circulating $t_{1/2}$ in general, they may be suitable candidates for Fc fusion. In the literature, Fc-fusion proteins with IL-2, IL-12, and IL-15 were reported for the $t_{1/2}$ extension and antitumor activities (Zhu et al., 2015; Rhode et al., 2016; Vazquez-Lombardi et al., 2017; Jung et al., 2018).

The objectives of the research were to evaluate the pharmacokinetics (PK) of IL-10 Fc-fusion proteins (Fig. 1) and investigate the cause of nonlinear PK and a short $t_{1/2}$ (~1 day) observed at pharmacologically active doses. Specifically, target-mediated drug disposition (TMDD), commonly observed with monoclonal antibodies (mAb) against membrane-bound receptors (An, 2020), was examined for the role in the PK of Fc–IL-10 fusion proteins. Experiments were conducted to compare the PK of recombinant IL-10 versus those of Fc-fusion proteins. Changes in PK were evaluated in the presence of an IL-10 receptor alpha-blocking mAb and with an Fc-fusion protein that had a reduced receptor binding affinity. Additionally, compartmental analyses were conducted to quantitatively integrate the PK data. The findings from this work offered insights into the future drug design of using Fc for the $t_{1/2}$ extension.

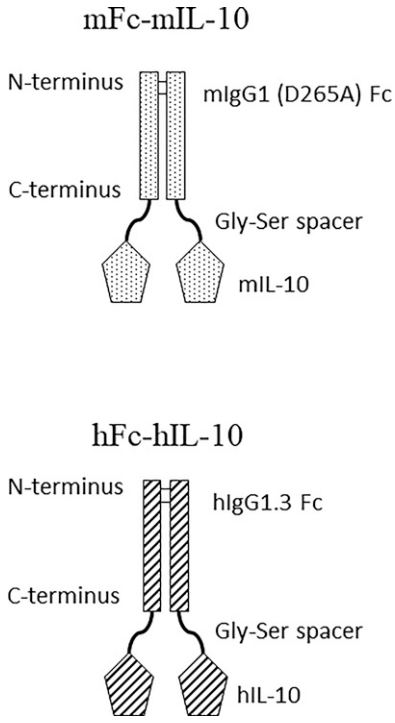

Fig. 1. Schematic structures of mFc–mIL-10 and hFc–hIL-10. Mutations were included in the Fc domains to eliminate or reduce antibody-dependent cellular cytotoxicity and complement-dependent cytotoxicity. For mFc–mIL-10, the Fc domain of murine immunoglobulin G1 (IgG1) had a single amino acid substitution of aspartic acid to alanine at codon 265 (D265A). For hFc–hIL-10, the Fc domain of human IgG1 (known as IgG1.3f) had three amino acid substitutions [leucine to alanine at codon 234 (L234A), leucine to glutamic acid at codon 235 (L235E), and glycine to alanine at code 237 (G237A)]. Both mouse IL-10 (mIL-10) and human IL-10 (hIL-10) were wild type and fused with the C terminus of the Fc domain through a glycine-serine rich polypeptide linker to retain the activity of IL-10. The sequence structures and characterizations are available in Supplemental Material.

Materials and Methods

Materials and Reagents

Mouse IL-10 (mIL-10), human IL-10 (hIL-10), mouse Fc–mouse IL-10 (mFc–mIL-10), human Fc–human IL-10 (hFc–hIL-10), and hFc–hIL-10 with a reduced target binding affinity (hFc–hIL-10 mutant) were produced at Bristol Myers Squibb. Recombinant human IL-10 receptor alpha protein, biotinylated mouse anti–human immunoglobulin G (IgG) Fc mAb, and mouse anti–mouse programmed death-1 (mPD-1) IgG1 mAb with a single amino acid substitution of aspartic acid to alanine at codon 265 (D265A) were also generated at Bristol Myers Squibb. Recombinant mouse IL-10 receptor alpha protein was obtained from R&D systems (Minneapolis, MN). Rat anti–mouse IL-10 biotinylated antibody, rat anti–human IL-10 antibody, and goat anti–mouse IgG antibody labeled with Alexa Fluor 647 were purchased from Southern Biotech (Birmingham, AL). Rat anti–mIL-10 receptor alpha mAb 1B1.3A was obtained from Bio X Cell (Lebanon, NH). All other reagents were obtained from commercial sources in analytical grade.

In Vitro Studies

Determination of Binding Affinity. The binding affinity, measured as the equilibrium dissociation constant (K_d), was determined using a surface plasmon resonance (SPR) method. For the IL-10 receptor alpha K_d determination, the experiments were conducted at 25°C using the Biacore T200 biosensor system (Cytiva, Marlborough, MA). The drug molecules (mFc–mIL-10 or hFc–hIL-10) were either directly immobilized on a CM5 chip (Cytiva), using 1-ethyl-3-(3-dimethylaminopropyl)carbodiimide hydrochloride (EDC)/N-hydroxysuccinimide (NHS) to a density of roughly 300 resonance units (RU) or captured to a Protein A Series S chip (Cytiva), at 2 μg/ml using 30-second contact time at a flow rate of 10 μl/min to give approximately 200–300 RU. An mIL-10 receptor alpha solution was prepared in a buffer (pH 7.2) containing phosphated-buffered saline and 0.05% Tween 20 (PBS-T) (Teknova Inc., Hollister, CA) at concentrations of 0.82, 2.5, 7.4, 22.2, 66.6, and 200 nM. Similarly, an hIL-10 receptor alpha solution was prepared in the same buffer at concentrations of 4.1, 12.3, 37.0, 111, 333, and 1000 nM. Protein solutions were then injected for 3 minutes at a flow rate of 30 μl/min followed by 5 minutes of dissociation using the "high performance" sample injection type in the Biacore T200 Software Method Builder. The

immobilized surface was regenerated back to baseline using a 60-second injection of 2M $MgCl_2$ followed by a 60-second injection of 20 mM ethylenediamine tetraacetic acid (EDTA). The protein A surface was regenerated back to the baseline using two 15-second injections of a glycine solution at pH 1.5. The K_d was estimated by a global fitting of the data using either the 1:1 Langmuir binding model or the steady-state affinity model available in the Biacore T200 Software.

To determine the neonatal Fc receptor (FcRn) K_d of hFc–hIL-10, SPR studies were conducted on a Biacore 8K biosensor system (Cytiva). A series S CM5 sensor chip was equilibrated with PBS-T pH 7.2 SPR running buffer at 25°C, and then hFc–hIL-10 was immobilized by diluting in acetate pH 4.5 and coupling using standard EDC/NHS chemistry with ethanolamine blocking. The immobilization level obtained was 330 RU for hFc–hIL-10. After priming the system, the binding of human and mouse FcRn analytes was tested by titrating an increasing concentration series of 19.5, 39.1, 78.1, 156, 313, 625, 1250, 2500, 5000, and 10,000 nM FcRn in PBS-T pH 6.0, as well as a single 2500 nM FcRn injection in PBS-T pH 7.4 to confirm lack of binding at neutral pH. All binding studies were done with association and dissociation times of 180 seconds each at a flow rate of 30 μl/min. The immobilized surface was regenerated back to baseline using 2 × 30s injections of Tris pH8 + 150mM NaCl. The K_d was estimated by a global fitting of the data using either the 1:1 Langmuir binding model or the steady-state affinity model available in the Biacore Insight Evaluation Software.

Evaluation of Cellular Activity. The cellular activity of mFc–mIL-10 and hFc–hIL-10 was evaluated in primary T cells by measuring the phosphorylation of STAT3, a downstream signal of the IL-10 receptor alpha activation. For the mouse assay, splenocytes from C57/BL6 mice were used in the studies. Briefly, spleens pooled from mice were manually dissociated and made into single-cell suspension by mechanical disruption and filtering through a 70-μM filter followed by red blood cell lysis for 3 minutes at 37°C. After lysis, cells were washed with phosphate-buffered saline (PBS) (Thermo Fisher Scientific, Waltham, MA), resuspended in complete media [Roswell Park Memorial Institute (RPMI) 1640, 10% fetal bovine serum, and 0.05 mM 2-mercaptoethanol] and plated at 5×10^5 cells per well in a 96-well plate. After a 1-hour rest, mFc–mIL-10 or controls were added to the wells and incubated for 15 minutes at 5% CO_2 at 37°C. The stimulation was stopped using cold fluorescence-activated cell sorting (FACS) buffer (0.5% fetal bovine serum in PBS), and cells were washed with FACS buffer and fixed using BD Cytofix (BD Biosciences, Franklin Lakes, NJ) on ice for 20 minutes before resuspension in cold Phosflow Perm Buffer III (BD Biosciences). Samples were subsequently stored at −20°C until staining. After overnight incubation at −20°C, samples were washed twice with FACS buffer and resuspended in 100 μl FACS buffer. Aliquots of samples in 50 μl were transferred to 96-well U-Bottom plates and treated with a blocking reagent (BD mouse FC block; BD Biosciences) at room temperature for 10 minutes followed by incubation with antibodies for surface and internal markers. For cluster of differentiation 3 (CD3), fluorescein isothiocyanate (FITC)-labeled anti–mouse CD3 antibody (BD Biosciences) was used. For phosphorylated STAT3, a mouse anti–STAT3-PE (pY705) antibody (BD Biosciences) was employed. After a 30-minute incubation at room temperature, samples were washed twice with 200 μl FACS buffer, centrifuged at 1500 rpm for 5 minutes, and resuspended in 150 μl FACS buffer. The samples were then analyzed by a FACSCanto X-20 flow cytometer (BD Biosciences).

For the human assay, whole blood obtained from human healthy donors (N = 3) was used in the experiments. Whole blood samples were drawn in heparin tubes and rested for 1 hour at 37°C in 5% CO_2. hFc–hIL-10 or controls were added to 100 μl of blood in 96-well plates and incubated for 15 minutes with 5% CO_2 at 37°C. After incubation, 1.7 ml of Phosflow Lyse/Fix buffer (BD Biosciences) was added to each sample and incubated for 10 minutes at 37°C to fix lymphocytes and lyse red blood cells. Cells were washed one time in FACS buffer and stained for CD3 using an allophycocyanin-labeled anti-CD3 antibody (BioLegend, San Diego, CA) and washed again in FACS buffer before resuspension in 1 ml of cold Phosflow Perm Buffer III (BD Biosciences). Samples were subsequently stored at −20°C. After overnight incubation at −20°C, samples were washed twice with FACS buffer and resuspended in 100 μl FACS buffer. Samples were then stained with antibodies for phosphorylated STAT3 using the mouse anti–STAT3-PE (pY705) antibody. After a 30-minute incubation at room temperature, samples were washed twice with 200 μl FACS buffer, centrifuged at 1500 rpm for 5 minutes, and resuspended in 150 μl FACS buffer. The samples were then analyzed by the FACSCanto X-20 flow cytometer.

In Vivo Studies

All studies were conducted according to the study protocols approved by the Bristol Myers Squibb Institutional Animal Care and Use Committee. Animals were acclimated for 7–17 days before the studies and had free access to food and water ad libitum. Female mice were used in antitumor efficacy studies for practical and compassionate reasons because they are easier to handle than male mice and can be housed together. Additionally, sex differences in immune responses were reported in the literature (Ray et al., 2020). Having mice of the same sex reduced study variability. Consistent with efficacy evaluations, PK studies were also performed in the same sex of mice.

Exposure to mFc–mIL-10 in Efficacy Evaluations. Systemic exposure to mFc–mIL-10 was evaluated from several efficacy studies conducted in the mouse MC38 and CT26 syngeneic tumor models. Tumor cells (1 million) suspended in sterile Hanks' balanced salt solution were subcutaneously implanted on the right flank of animals. Dosing was typically initiated 7 days after reaching a mean tumor volume of 100 mm^3 and randomizing animals into treatment groups. Mice were weighed immediately after randomization (before administration of treatment) and at least twice weekly through day 28. The measurement of tumor volume throughout the study was determined by a caliper and recorded twice weekly until all tumors reached either tumor burden or had completely regressed. Tumor burden was identified as a tumor reaching or exceeding 1000 mm^3 for two consecutive measurements or exceeding 2000 mm^3 at any one measurement. Animals that had their tumors completely regressed were palpated weekly to confirm tumor rejection.

mFc–mIL-10 was evaluated as a single agent for antitumor efficacy in the mouse MC38 syngeneic tumor model (female C57BL6 mice, ∼20 g; Charles River Laboratories, Wilmington, MA). Two efficacy studies were conducted. The drug was formulated in PBS and given as a single dose intraperitoneally (i.p.) to mice at a dosing volume of 10 ml/kg. The doses studied were 0.1, 0.3, 1, 3, and 10 mg/kg, with 10 mice per dose group along with an isotype control group. In one of the efficacy studies, systemic exposure to mFc–mIL-10 was obtained from tumor-bearing mice, in which serial blood samples of 60 μl were obtained via submandibular bleeds at 4 and 168 hours after the dose, with five mice per time point. Submandibular bleeds were performed with the use of a sterile 5-mm Goldenrod animal lancet (Braintree Scientific Inc., Braintree, MA). Animals were briefly restrained, and an applicable volume of blood was collected from a puncture made proximal of the mandibular bone where the submandibular vein and the facial vein converge. Additionally, as part of the efficacy experiment, a dedicated PK evaluation with mFc–mIL-10 was conducted in the satellite groups of non–tumor-bearing mice at the doses of 0.3 and 3 mg/kg i.p., in which blood samples (60 μl) were harvested via submandibular bleeds at 1, 5, 24, 72, 168, 240, and 336 hours postdose in a composite fashion, with three mice per time point. After the blood sample collection at each time point, serum samples were harvested and stored at ≤−70°C until sample analysis for mFc–mIL-10 concentrations.

In the mouse CT26 syngeneic tumor model (female BALB/c mice, ∼20 g; Envigo, Indianapolis, IN), the antitumor efficacy of mFc–mIL-10 was evaluated in combination with a mouse anti–mPD-1 mAb in three experiments. The anti–mPD-1 mAb was administered every 4 days at 10 mg/kg i.p. for three doses, whereas mFc–mIL-10 was given as a single i.p. injection. The doses of mFc–mIL-10 in the first study were 0.1, 0.3, and 1 mg/kg. They were 0.1 and 0.3 mg/kg in the second study and 0.03, 0.1, and 0.3 mg/kg in the third study. Eight or ten mice were studied at each dose level along with isotype control and an anti–mPD-1 monotherapy group. Blood samples (10 μl) were obtained compositely in the first study and serially in the second and third studies. They were collected by microsampling on the tail vein from tumor-bearing mice at 4, 24, 48, 96, 168, 192 (or 216), 336, and 504 hours postdose, with four or six mice per time point. After the blood sample collections at each time point, they were diluted with 90 μl Rexxip A buffer (Gyros AB, Uppsala, Sweden) and stored at ≤−70°C until sample analysis for mFc–mIL-10 concentrations.

Intravenous Pharmacokinetic Studies with mFc–mIL-10 and hFc–hIL-10. Pharmacokinetic studies were conducted in nonfasted female C57BL6 mice (20–25 g; Charles River Laboratories) after intravenous (i.v.) administration at the doses of 0.05, 0.5, and 5 mg/kg. At each dose, four mice received either mFc–mIL-10 or hFc–hIL-10 that was formulated in PBS at a dosing volume of 5 ml/kg. Serial blood samples (10 μl) were obtained by microsampling on the tail vein at predose, 0.05, 1, 3, 5, 7, 24, 48, 72, 96, 168, and 240 hours postdose and diluted with 90 μl Rexxip A buffer. At the end of the studies,

serum samples (30–50 μl) were also collected via cardiac puncture. Samples were stored at $\leq -70°C$ until analysis for mFc–mIL-10 or hFc–hIL-10 concentrations.

Intravenous Pharmacokinetic Studies with mIL-10 and hIL-10. Pharmacokinetic studies were conducted in nonfasted female C57BL6 mice (20–25 g; Charles River Laboratories) after i.v. administration at the doses of 0.05, 0.5, and 5 mg/kg. At each dose, four mice received either mIL-10 or hIL-10 that was formulated in PBS at a dosing volume of 5 ml/kg. Serial blood samples (10 μl) were harvested by microsampling on the tail vein at predose, 0.05, 0.5, 1, 5, 7, and 24 hours postdose and diluted with 90 μl Rexxip A buffer. At the end of the studies, serum samples (30–50 μl) were also collected via cardiac puncture. Samples were stored at $\leq -70°C$ until analysis for mIL-10 or hIL-10 concentrations.

Intraperitoneal Pharmacokinetic Study with mFc–mIL-10 in Presence and Absence of Rat Anti–mIL-10 Receptor Alpha Antibody. Nonfasted female BALB/c mice (20–25 g; Charles River Laboratories) were used in the study. The rat anti–mIL-10 receptor alpha antibody was administered subcutaneously 1 day before the dosing of mFc–mIL-10. The intended doses for the anti–mIL-10 receptor alpha antibody were 5 and 50 mg/kg. Due to a limited quantity of the dosing solutions, two mice in the 5-mg/kg group received the full dose, whereas the third mouse was given a dose of 3.5 mg/kg. In the 50-mg/kg group, two mice received the full dose, and the third mouse was dosed at 13 mg/kg. Additionally, PBS as the vehicle for the anti–mIL-10 receptor alpha antibody was given to four mice as the control group. One day after the subcutaneous administration of the anti–mIL-10 receptor alpha antibody, mFc–mIL-10 formulated in PBS was administered i.p. at a dose of 0.1 mg/kg, with a dosing volume of 5 ml/kg. Serial blood samples (10 μl) were obtained by microsampling on the tail vein at predose, 4, 24, 48, 72, 79, 144, and 168 hours postdose and diluted with 90 μl Rexxip A buffer. At the end study, serum samples (30–50 μl) were also collected via cardiac puncture. Samples were stored at $\leq -70°C$ until analysis for mFc–mIL-10 concentrations.

Intraperitoneal Pharmacokinetic Studies with hFc–hIL-10 and hFc–hIL-10 Mutant. hFc–hIL-10 or hFc–hIL-10 mutant, formulated in PBS at a dosing volume of 5 ml/kg, was given to four nonfasted female BALB/c mice (20–25 g; Charles River Laboratories) at a dose of 0.1 mg/kg. Serial blood samples (10 μl) were collected by microsampling on the tail vein at predose, 4, 24, 48, 72, 79, 144, and 168 hours postdose and diluted with 90 μl Rexxip A buffer. At the end study, serum samples (30–50 μl) were also collected via cardiac puncture. Samples were stored at $\leq -70°C$ until analysis for hFc–hIL-10 and hFc–hIL-10 mutant concentrations.

Sample Analysis

Quantitation of mFc–mIL-10. The concentrations of mFc–mIL-10 in mouse samples (10% blood in Rexxip A buffer or serum) were measured using a microfluidic fluorescence immunoassay on a Gyrolab xP Workstation (Gyros AB). A biotinylated rat anti–mIL-10 antibody (Southern Biotech) was used as the capture reagent, and a goat anti–mIgG antibody labeled with Alexa Fluor 647 (Southern Biotech) was used as the detection reagent. For diluted blood samples (10% blood in Rexxip A buffer), standard curves and quality control (QC) samples defining the dynamic range of the bioanalytical method were prepared in the 10% mouse blood with Rexxip A buffer and processed in the same fashion as the test samples. For serum samples, they were analyzed at 5-fold dilution in PBS with 1% bovine serum albumin (BSA) and 1M sodium chloride; the corresponding standard and QC samples were prepared in the same way as the serum test samples. Aliquots of diluted test samples, QC samples, standards, and reagents were added to 96-well polymerase chain reaction (PCR) microplates (Thermo Fisher Scientific, Cambridge, MA). The Gyrolab workstation transferred samples and reagents from the microplates to each of the microstructures within a Gyrolab Bioaffy compact disc (CD) and spun each CD at the optimized speed and time controlled by the Gyros software to ensure uniform optimal reaction times throughout the integrated assay workflow. All assay steps were automated and controlled by the Gyros control software. The mFc–mIL-10 concentrations in the test samples were quantified by a log-log linear-fit regression model using the SoftMax Pro software (Molecular Devices, Sunnyvale, California). Standard curves and QC samples were evaluated using target acceptance criteria for inaccuracy and imprecision of ±20% of the nominal concentration to be considered acceptable for assay performance. The lower limit of quantitation (LLOQ) in diluted blood and serum samples were 0.4 and 3 ng/ml (0.004 and 0.03 nM), respectively. The LLOQ in plasma after the conversion of drug concentrations from diluted blood samples using a theoretical dilution factor of 17.36 (see *Data Analysis* for details) was 6.9 ng/ml (0.08 nM).

Quantitation of hFc–hIL-10 and hFc–hIL-10 Mutant. The concentrations of hFc–hIL-10 and hFc–hIL-10 mutant in mouse samples (10% blood in Rexxip A buffer or serum) were measured using a chemiluminescence immunoassay platform developed at Bristol Myers Squibb. A rat anti–hIL-10 (Southern Biotech) and biotin-labeled mouse anti–human IgG Fc antibody (produced at Bristol Myers Squibb) were used as the capture and detection reagents, respectively. For diluted blood samples (10% blood in Rexxip A buffer), standard curves and QC samples defining the dynamic range of the bioanalytical method were prepared in the 10% mouse blood with Rexxip A buffer and processed in the same fashion as the test samples. Serum samples were analyzed in Rexxip buffer A and loaded in the capture reagent coated, blocked 96-well flat-bottom Nunc MaxiSorp black plate (Thermo Fisher Scientific, Waltham, MA). After the incubation and wash step, the detection reagent, an in-house biotin-labeled mouse anti–human IgG Fc antibody, was added. After another incubation and wash step, NeutrAvidin protein conjugated with horseradish peroxidase (Thermo Fisher Scientific, Waltham, MA) was added. After the final incubation and wash step, Pico substrate solution (Thermo Fisher Scientific, Waltham, MA) was added to assay plates and read in SpectraMax plate reader at the luminescence mode. Calibrators and QCs were analyzed on each assay plate along with samples to ensure acceptable assay performance. The concentrations of hFc–hIL-10 or hFc–hIL-10 mutant in mouse serum samples were calculated from the luminescence intensity using a log-log linear calibration curve. Assay performance was within the acceptable range: % CV of the standards and QC was below 20%, and QC recovery was within ±20% of the nominal values. The LLOQs of hFc–hIL-10 in diluted blood and serum samples were 0.4 and 1 ng/ml (0.004 and 0.01 nM), respectively. The corresponding LLOQ in plasma after the conversion of drug concentrations from diluted blood samples using the theoretical dilution factor of 17.36 (see *Data Analysis* for details) was 6.9 ng/ml (0.08 nM). The LLOQs of the hFc–hIL-10 mutant in diluted blood and serum samples were 2.5 and 2.5 ng/ml (0.03 nM), respectively. The corresponding LLOQ of the hFc–hIL-10 mutant in plasma after the correction from diluted blood samples was 43 ng/ml (0.5 nM).

Quantitation of mIL-10. The concentrations of mIL-10 in mouse samples (10% blood in Rexxip A buffer or serum) were measured using the same procedure as described above for mFc–mIL-10, except that a rat anti–mIL-10 antibody labeled with Alexa Fluor 647 (Southern Biotech) was used as the detection reagent. The LLOQs in diluted blood and serum samples were 0.025 and 1 ng/ml (0.0007 and 0.03 nM), respectively. The corresponding LLOQ in plasma after the correction from diluted blood samples was 0.4 ng/ml (0.01 nM).

Quantitation of hIL-10. The concentrations of hIL-10 in mouse samples (10% blood in Rexxip A buffer or serum) were measured using the same procedure as described above for mFc–mIL-10, except that a biotinylated rat anti–hIL-10 antibody (Southern Biotech) and a rat anti–hIL-10 antibody labeled with Alexa Fluor 647 (Southern Biotech) were used as the capture and detection reagents, respectively. The LLOQs in diluted blood and serum samples were 0.25 and 0.25 ng/ml (0.007 nM), respectively. The corresponding LLOQ in plasma after the correction from diluted blood samples was 4 ng/ml (0.1 nM).

Data Analysis

Data are expressed as mean ± standard deviation (S.D.). For Rexxip A buffer-diluted blood samples collected in mice, a theoretical dilution factor of 17.36 was used for correcting the drug levels to undiluted plasma drug concentrations (Joyce et al., 2014). The theoretical dilution factor was determined by assuming that the biotherapeutic agents such as recombinant IL-10 and associated Fc-fusion proteins largely reside in the plasma volume. A dilution of 10 μl of blood into 90 μl Rexxip A buffer dilutes the drugs residing in 5.5 μl of plasma water, assuming a hematocrit value of 0.45. As a result, the theoretical dilution factor is calculated as the sum of 90 μl buffers and 5.5 μl plasma water divided by 5.5 μl plasma water ($95.5 \div 5.5 = 17.36$).

Noncompartmental Pharmacokinetic Analysis. The pharmacokinetic parameters were obtained by noncompartmental analysis of plasma concentration versus time data using PKSolver (Zhang et al., 2010). The peak concentration (C_{max}) and time for C_{max} (T_{max}) were recorded directly from experimental observations. The area under the curve from time zero to infinity (AUC_{tot}) was calculated using a combination of linear and log trapezoidal summations. The total

plasma clearance (CL_{tot}), steady-state volume of distribution (V_{ss}), and terminal $t_{1/2}$ were estimated after i.v. administration.

Compartmental Pharmacokinetic Analysis. The i.v. PK data were fitted with a two-compartment model. To fit the mFc–mIL-10 and hFc–hIL-10 data, target- and nontarget-mediated elimination was incorporated into the two-compartment model. The differential equations are shown below:

$$V_c \frac{dC_P}{dt} = A_{peripheral} \times k_{21} - \left(k_{el,\,nontarget-mediated} + k_{12} + \frac{V_{max,\,target-mediated}}{K_{m,\,target-mediated} \times V_c + V_c \times C_p}\right) \times V_c \times C_p \quad (1)$$

$$\frac{dA_{peripheral}}{dt} = k_{12} \times V_c \times C_p - k_{21} \times A_{peripheral} \quad (2)$$

where $A_{peripheral}$ is the drug amount in the peripheral compartment; C_p is the drug concentration in the central compartment; V_c is the volume of distribution in the central compartment; k_{12} is the transfer rate constant from the central to peripheral compartment; k_{21} is the transfer rate constant from the peripheral to the central compartment; $k_{el,nontarget\text{-}mediated}$ is the nontarget-mediated first-order elimination rate constant; $V_{max,target\text{-}mediated}$ is the maximum elimination rate mediated by a target; and $K_{m,target\text{-}mediated}$ is the binding affinity to the target. For mIL-10 and hIL-10, only nontarget-mediated elimination was needed to fit the i.v. PK data. With eq. 2 remaining the same, eq. 1 becomes:

$$V_c \frac{dC_P}{dt} = A_{peripheral} \times k_{21} - (k_{el,\,nontarget-mediated} + k_{12}) \times V_c \times C_p \quad (3)$$

At time zero, the following initial condition exists for i.v. administration:

$$C_{p,\,t=0} = \frac{Dose_{IV}}{V_c} \quad (4)$$

$$A_{peripheral,\,t=0} = \cdot 0 \quad (5)$$

where $Dose_{IV}$ is the i.v. dose administered. It is worth noting that it was necessary to consider nonspecific drug adsorption to devices during dosing solution preparations and actual dosing at the low i.v. dose of 0.05 mg/kg. Otherwise, the concentrations at 0.05 mg/kg predicted by the PK model were consistently higher than the observed values. In contrast, the phenomenon was not evident at two higher doses of 0.5 and 5 mg/kg. As a result, the initial condition for $C_{p,t=0}$ at 0.05 mg/kg was equal to:

$$C_{p,\,t=0,\,at\ 0.05\,mg/kg} = \frac{Dose_{IV} \times \%remaining}{V_c} \quad (6)$$

where % remaining is the percentage of the dose remaining after nonspecific drug adsorption and the value was estimated from the PK model.

To model the mFc–mIL-10 i.p. PK data, the first-order absorption coupled with the two-compartment model was employed. The differential equations are given below:

$$\frac{dA_{IP}}{dt} = -k_a \times A_{IP} \quad (7)$$

$$V_{c,apparent} \frac{dC_P}{dt} = k_a \times A_{IP} + A_{peripheral} \times k_{21} - \left(k_{el,\,nontarget-mediated} + k_{12} + \frac{V_{max,\,target-mediated}}{K_{m,\,target-mediated} \times V_{c,apparent} + V_{c,apparent} \times C_p}\right) \times V_{c,apparent} \times C_p \quad (8)$$

$$\frac{dA_{peripheral}}{dt} = k_{12} \times V_{c,apparent} \times C_p - k_{21} \times A_{peripheral} \quad (9)$$

where A_{IP} is the amount of the drug at the i.p. absorption site, k_a is the absorption rate constant, and $V_{c,apparent}$ is the apparent volume of distribution in the central compartment after i.p. administration. In this case, the $V_{c,apparent}$, as opposed to the i.p. bioavailability, was used as a parameter to model the data after i.p. administration. It was because the i.p. bioavailability estimated from the simultaneous fitting of the mFc–mIL-10 i.v. and i.p. data was >100% across a wide dose range (0.03–3 mg/kg), indicating a systematic difference between the i.v. and i.p. studies. Therefore, the $V_{c,apparent}$ was used as a scalar to fit the i.p. data and avoid the wrong impression that the i.p. bioavailability of mFc–mIL-10 was >100%.

At time zero, the following conditions exist:

$$A_{IP,\,t=0} = Dose_{IP} \quad (10)$$

$$C_{P,\,t=0} = 0 \quad (11)$$

$$A_{peripheral,\,t=0} = \cdot 0 \quad (12)$$

where $Dose_{IP}$ is the dose administered via the i.p. route. Same as the i.v. PK data modeling, the nonspecific drug adsorption to devices needed to be considered for the low i.p. dose of 0.03 mg/kg but not for higher doses. Consequently, the initial condition for $A_{IP,t=0}$ at the 0.03-mg/kg i.p. dose was equal to:

$$A_{Ip,\,t=0,\,at\,0.03\,mg/kg} = Dose_{Ip} \times \%remaining \quad (13)$$

For the mFc–mIL-10 i.p. PK data, they were simultaneously fitted together with the i.v. data to obtain one set of parameters, except for V_c, $V_{c,apparent}$, and k_a.

The compartmental PK analysis was conducted using SAAM II (v2.3.1.1; The Epsilon Group, Charlottesville, VA) to describe the average PK data across the dose range evaluated. The weighting function was 1/y. The goodness of fit was assessed by the minimization of the objective function, Akaike and Schwarz-Bayesian information criteria, visual inspection of the fitting and residual plots, and the precision of the parameters estimated.

Statistical Analysis. Student's *t* test was used. A difference was considered significant when the *P* value was <0.05.

TABLE 1

Molecular mass, binding affinity, and cellular activities of mFc–mIL-10 and hFc–hIL-10

	mFc–mIL-10	hFc–hIL-10
Molecular Mass (Dalton)	91,004	90,815
Binding Affinity (nM)[a]		
Mouse IL-10 receptor alpha	3.2	2.9
Human IL-10 receptor alpha	No binding	0.6
Mouse neonatal Fc receptor	640[b]	200
Human neonatal Fc receptor	No binding	1,100
In Vitro Cellular Activity (nM)		
STAT3 phosphorylation in mouse CD3+ T cells	0.44	0.55
STAT3 phosphorylation in human CD3+ T cells	Not tested	0.24

[a]Determined at 25°C and pH 7.2 for mouse and human IL-10 receptor alpha and 25°C and pH 6.0 for mouse and human neonatal Fc receptor.
[b]Wang et al. (2020).

Results

Properties of mFc–mIL-10 and hFc–hIL-10. Table 1 summarizes the various properties of mFc–mIL-10 and hFc–hIL-10, with the sequence structures and additional characterization information available in Supplemental Material. The molecular masses of both molecules were about 90 kDa, and they had a comparable binding affinity K_d (~3 nM) to mIL-10 receptor alpha. The K_d of hFc–hIL-10 toward hIL-10 receptor alpha was 0.6 nM, comparable to that (0.05–0.5 nM) of hIL-10 reported in the literature (Moore et al., 2001; Walter, 2014). The cellular activity in mouse and human CD3+ T cells was also in the same range for both agents (Table 1). These results confirm that hFc–hIL-10 cross-reacts to mIL-10 receptor alpha. mFc–mIL-10 had the Fc domain of IgG1 with a single amino acid substitution of aspartic acid to alanine at codon 265 (D265A). The K_d of mFc–mIL-10 to the mouse

neonatal Fc receptor (FcRn) was previously reported to be 640 nM (Wang et al., 2020). In comparison, hFc–hIL-10 carried the Fc domain of human IgG1 with three amino acid substitutions [leucine to alanine at codon 234 (L234A), leucine to glutamic acid at codon 235 (L235E), and glycine to alanine at code 237 (G237A)] to reduce the effector function. The K_d of hFc–hIL-10 to the mouse and human FcRn was determined to be 200 and 1100 nM, respectively (Table 1). The results are consistent with the literature findings in which human IgG antibodies are found to have a tighter binding affinity to mouse FcRn than to human (Abdiche et al., 2015).

Systemic Exposure to mFc–mIL-10 after Intraperitoneal Administration in Efficacy Evaluations. mFc–mIL-10 was pharmacologically active in the mouse syngeneic models after a single i.p. dose injection. In the MC38 mouse tumor model, the percentage of mice that were tumor-free at the doses of 0.1, 0.3, 1, 3, and 10 mg/kg, averaged from two antitumor efficacy studies, was 5%, 65%, 95%, 90%, and 90%, respectively. In the CT26 mouse tumor model, mFc–mIL-10 was efficacious when combined with an anti–mPD-1 mouse surrogate; the percentage of mice without tumors at the doses of 0.03, 0.1, 0.3, and 1 mg/kg averaged from three studies was 40, 77, 85, and 100%, respectively, compared with 14% of animals receiving only the anti–mPD-1 mAb. These data indicate that mFc–mIL-10 was pharmacologically active at doses of ≥0.1 mg/kg.

In the efficacy studies, the systemic exposure to mFc–mIL-10 after i.p. administration was also examined. Figure 2A shows the plasma concentration-time profiles of mFc–mIL-10 at the dose range of 0.03–3 mg/kg. With a nominal dose ratio of 1:3:10:33:100 and a nonspecific adsorption-corrected dose ratio of 1:8.8:26:88:263, the C_{max} and AUC_{tot} ratios were 1:11:46:189:556 and 1:14:56:283:937, respectively (Table 2). The terminal $t_{1/2}$ also increased with the doses. Moreover, at the pharmacologically active doses of 0.1–0.3 mg/kg, the terminal $t_{1/2}$ was 1.2–1.5 days, significantly shorter than typical mouse IgG1 $t_{1/2}$ of 6–8 days (Vieira and Rajewsky, 1988).

mFc–mIL-10 and hFc–hIL-10 Pharmacokinetics after Intravenous Administration to Mice. To investigate the nonlinear PK observed in the efficacy evaluations after i.p. dosing, mFc–mIL-10 and hFc–hIL-10 were administered i.v. to non–tumor-bearing mice at the doses of 0.05, 0.5, and 5 mg/kg. Table 3 summarizes the PK parameters of mFc–mIL-10 and hFc–hIL-10 estimated using noncompartmental analysis. Figure 2, B and C depicts the plasma concentration-time profiles after i.v. administration. Similar to the results from the i.p. dosing, mFc–mIL-10 exhibited a significant nonlinear PK after i.v. administration. With a nominal dose ratio of 1:10:100 and a nonspecific adsorption-corrected dose ratio of 1:28:278, the C_{max} and AUC_{tot} ratios were 1:28:263 and 1:181:1830, respectively (Table 3). The CL_{tot} decreased from 239 to 33 ml/day/kg when the dose increased from 0.05 to 5 mg/kg. These clearance values appear to be higher than the clearance data (~10 ml/day/kg) commonly observed with mAb in mice without TMDD (Betts et al., 2018). The V_{ss} showed an increasing trend with the dose but was still in a range comparable to the values (~60–130 ml/kg; Betts et al., 2018) of mAb, which has a larger molecular mass than that of mFc–mIL-10. Because of dose-dependent changes in the CL_{tot} and V_{ss}, the terminal $t_{1/2}$ values at 0.05, 0.5, and 5 mg/kg were 0.22, 2.6, and 3.9 days, respectively. These results indicate that the disposition of mFc–mIL-10 was nonlinear.

Like mFc–mIL-10, hFc–hIL-10 exhibited a nonlinear PK after i.v. administration. With a nominal dose ratio of 1:10:100 and a nonspecific adsorption-corrected dose ratio of 1:19:192, the C_{max} and AUC_{tot} ratios were 1:21:187 and 1:75:633, respectively (Table 3). The CL_{tot} decreased with the dose (162 to 41 ml/day/kg), with the V_{ss} showing a slightly increasing trend (106 to 161 ml/kg). As a result, the terminal $t_{1/2}$ at 0.05, 0.5, and 5 mg/kg was 0.45, 2.5, and 2.0 days, respectively. Similar findings between mFc–mIL-10 and hFc–hIL-10 pointed to the direction of TMDD as the cause of nonlinear PK because both molecules had similar binding affinity values to mIL-10 receptor alpha (Table 1).

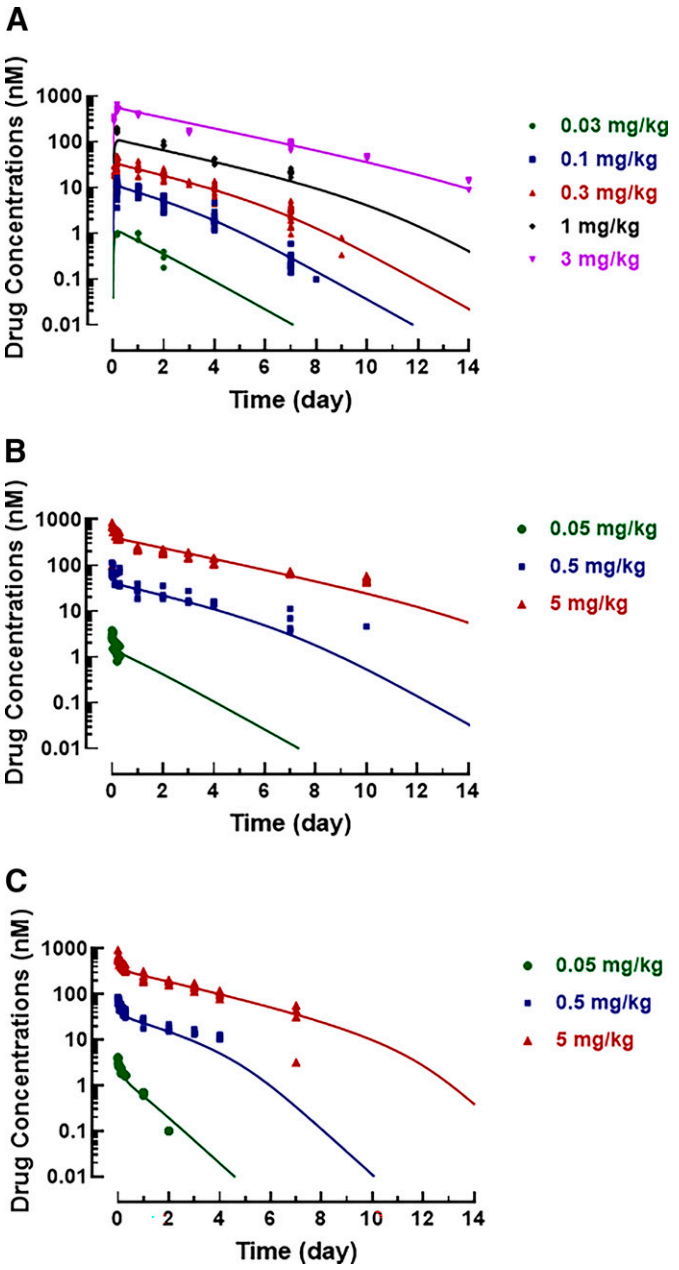

Fig. 2. Plasma (or serum) concentration-time profiles of mFc–mIL-10 and hFc–hIL-10 in mice. (A) Intraperitoneal administration of mFc–mIL-10 at 0.03, 0.1, 0.3, 1, and 3-mg/kg doses to tumor-bearing mice in efficacy evaluations (N = 3–14 per time point, including data at 0.3 and 3 mg/kg obtained from non–tumor-bearing mice in the satellite groups of efficacy studies); (B) Intravenous dosing of mFc–mIL-10 at 0.05, 0.5, and 5-mg/kg doses to non–tumor-bearing mice (N = 4 per time point); and c) intravenous administration of hFc–hIL-10 at 0.05, 0.5, and 5-mg/kg doses to non–tumor-bearing mice (N = 4 per time point). Lines represent pharmacokinetic model-fitted average concentration-time curves. Symbols show individual observed data. When data points are fewer than the number of animals indicated or not shown in the figure, drug concentrations are below the LLOQ (0.08 nM in plasma and 0.03 nM in serum for mFc–mIL-10; 0.08 nM in plasma and 0.01 nM in serum for hFc–hIL-10).

TABLE 2

Pharmacokinetic parameters of mFc–mIL-10 after intraperitoneal administration to tumor-bearing mice in efficacy studies
(Pharmacokinetic parameters were calculated based on the average concentration-time data from antitumor efficacy studies. Because a portion of the drug concentration data were obtained compositely, the standard deviation cannot be obtained for the pharmacokinetic parameters estimated.)

	0.03 mg/kg (N = 4)	0.1 mg/kg (N = 14)	0.3 mg/kg[a] (N = 12)	1 mg/kg (N = 4)	3 mg/kg[a] (N = 3)
C_{max} (nM)	0.9	10	41	170	500
C_{max} ratio[b]	1.0	11	46	189	556
T_{max} (h)	4	4	5	4	5
AUC_{tot} (nM*days)	1.8	25	100	509	1686
AUC_{tot} ratio[b]	1.0	14	56	283	937
Terminal $t_{1/2}$ (days)	1.0	1.2	1.5	2.2	2.7

[a]Pharmacokinetic data from non–tumor-bearing mice in the satellite groups of an efficacy study were also included in the analysis (please see text for details).
[b]The nominal dose ratio was 1:3.3:10:33:100; the nonspecific adsorption-corrected dose ratio was 1:8.8:26:88:263 (see Table 5 for % drug remaining in dosing solution at 0.03 mg/kg estimated from compartmental modeling).

mIL-10 and hIL-10 Pharmacokinetics after Intravenous Administration to Mice. To examine the role of the target in the nonlinear PK observed with Fc-fusion proteins, the PK of mIL-10 and hIL-10 was studied in non–tumor-bearing mice after i.v. administration. Figure 3 shows the plasma concentration-time profiles of mIL-10 and hIL-10 at the doses of 0.05, 0.5, and 5 mg/kg, with the PK parameters summarized in Table 4. In contrast to the nonlinear PK observed with the Fc-fusion proteins, mIL-10 and hIL-10 demonstrated linear PK after i.v. administration. Across the same dose range as that of the Fc-fusion proteins, the CL_{tot} and V_{ss} were largely dose independent (Table 3). The CL_{tot} of mIL-10 was similar to the value reported in the literature (Alvarez et al., 2012), whereas the CL_{tot} of hIL-10 was about 2-fold higher than that of mIL-10. The V_{ss} of mIL-10 and hIL-10 was in a range of 103–143 ml/kg and 77–207 ml/kg, respectively. These values are generally in line with the literature data (Huhn et al., 1996; Alvarez et al., 2012). The terminal $t_{1/2}$ was 1–1.5 hours, consistent with the expected $t_{1/2}$ values for cytokines. These data suggest that the cytokine PK behaved differently from that of the Fc-fusion proteins.

Compartmental Analysis of Pharmacokinetic Data of Fc-Fusion Proteins and Cytokines in Mice. To further gain insight into the PK behaviors of Fc-fusion proteins and their corresponding cytokines, compartmental analysis was conducted. Table 5 summarizes the estimated PK parameters, with model-fitted curves displayed in Figs. 2 and 3. For each molecule, the PK model, developed using one set of parameters, described the central tendency of the data across a wide dose range. The key models tested and testing performance measured as the objective function, Akaike information criterion, and Schwarz-Bayesian information criterion are shown in Supplemental Tables 1–4, with diagnostic plots displayed in Supplemental Figs. 1–4.

For mFc–mIL-10, the i.v. and i.p. data were simultaneously fitted. Because a systematic difference in drug concentrations was observed between the i.v. and i.p. routes, the $V_{c,apparent}$ as opposed to the i.p. bioavailability was used as a scalar to account for the apparent difference between the two routes of administration. The V_c after i.v. administration was estima-ted to be 35–81 ml/kg, whereas the $V_{c,apparent}$ after i.p. administration of mFc–mIL-10 was 45 ml/kg. The V_c values were comparable to what was reported for mAb (Betts et al., 2018).

For the elimination of Fc-fusion protein, TMDD was assumed in the PK model, and the Michaelis-Menten kinetics was used. The in vitro binding affinity to the mIL-10 or hIL-10 receptor alpha was used as the $K_{m,target\text{-}mediated}$ for the curve fitting. Using this approach, nonlinear PK associated with the Fc-fusion proteins was reasonably described. The $k_{el,nontarget\text{-}mediated}$ for mFc–mIL-10 and hFc–hIL-10 was 0.019 and 0.023 $hours^{-1}$, respectively, suggesting that differences in the FcRn K_d (640 vs. 200 nM) between mFc–mIL-10 and hFc–hIL-10 did not result in differences in the nontarget-mediated clearances. Based on these values, the $t_{1/2}$ for nontarget mediated pathways, calculated as $0.693/k_{el,nontarget\text{-}mediated}$, was ~34 hours, which is in line with the mouse $t_{1/2}$ (17 hours) observed with elastin-like polypeptides that had a molecular mass of 86 kDa (Kuna et al., 2018).

For recombinant IL-10 proteins, incorporating TMDD into the cytokine elimination did not improve the data fitting. A two-compartment PK model without TMDD was sufficient to explain the data (Supplemental Figs. 3 and 4; Supplemental Tables 3 and 4). The $k_{el,nontarget\text{-}mediated}$ estimated for mIL-10 and hIL-10 was 4.3 and 5.9 $hours^{-1}$, respectively. The corresponding CL_{tot} predicted from the PK model was 2.5 and 5.7 ml/min/kg, respectively. These clearance values are in the same order of magnitude as the glomerular filtration rate (14 ml/min/kg) in mice (Davies and Morris, 1993). Additionally, the terminal $t_{1/2}$ of mIL-10 and hIL-10 predicted from the PK model was 1.1 and 0.9 hours, respectively. The values are shorter than the mouse $t_{1/2}$ (4.7 hours) reported for

TABLE 3

Pharmacokinetic parameters of mFc–mIL-10 and hFc–hIL-10 after intravenous administration to non–tumor-bearing mice

	mFc–mIL-10 (Mean ± S.D., N = 4)			hFc–hIL-10 (Mean ± S.D., N = 4)		
	0.05 mg/kg[a]	0.5 mg/kg	5 mg/kg	0.05 mg/kg[a]	0.5 mg/kg	5 mg/kg
C_{max} (nM)[b]	3.0 ± 0.6	83 ± 23	789 ± 215	3.7 ± 0.5	77 ± 12	693 ± 168
C_{max} ratio[c]	1.0	28	263	1.0	21	187
AUC_{tot} (nM*days)	0.9 ± 0.3	164 ± 50	1651 ± 136	1.8 ± 0.1	135 ± 16	1,139 ± 221
AUC_{tot} ratio[c]	1.0	181	1830	1.0	75	633
CL_{tot} (ml/day/kg)	239 ± 65	36 ± 10	33 ± 2.6	162 ± 8.5	41 ± 4.8	50 ± 10
V_{ss} (ml/kg)	78 ± 19	124 ± 32	178 ± 28	106 ± 5.2	161 ± 50	141 ± 25
Terminal $t_{1/2}$ (days)	0.22 ± 0.018	2.6 ± 0.55	3.9 ± 0.47	0.45 ± 0.039	2.9 ± 1.1	2.0 ± 0.83

[a]The dose of 0.05 mg/kg was corrected for drug loss due to nonspecific adsorption in dosing vials and devices. The actual doses used for PK parameter estimations were 0.019 mg/kg for mFc–mIL-10 and 0.026 mg/kg for hFc–hIL-10. These doses were estimated using compartmental modeling (Table 5; please see text for additional details).
[b]First sampling time point (3 min) after an i.v. bolus dose.
[c]The nominal dose ratio was 1:10:100; the nonspecific adsorption-corrected dose ratios for mFc–mIL-10 and hFc–hIL-10 were 1:26:263 and 1:19:192, respectively.

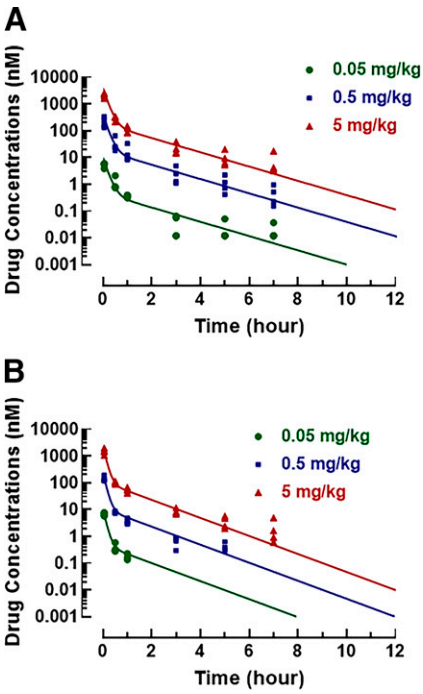

Fig. 3. Plasma concentration-time profiles of mIL-10 and hIL-10 in mice. (A) Intravenous dosing of mIL-10 at 0.05, 0.5, and 5-mg/kg doses to non–tumor-bearing mice ($N = 4$ per time point); (B) Intravenous administration of hIL-10 at 0.05, 0.5, and 5-mg/kg doses to non–tumor-bearing mice ($N = 4$ per time point). Lines represent pharmacokinetic model-fitted average concentration-time curves. Symbols show individual observed data. When data points are fewer than the number of animals indicated or not shown in the figure, drug concentrations are below the LLOQ (0.01 nM for mIL-10 and 0.1 nM for hIL-10).

elastin-like polypeptides that had the same molecular mass (37 kDa) as that of IL-10 (Kuna et al., 2018). It is possible that TMDD still exists for the cytokines but cannot be manifested readily due to a high nontarget-mediated clearance such as renal filtration.

mFc–mIL-10 Intraperitoneal Pharmacokinetics in Presence and Absence of Rat Anti–mIL-10 Receptor Alpha Antibody. To illustrate the role of TMDD in the PK of Fc-fusion proteins, the PK of mFc–mIL-10 was evaluated in the presence and absence of a rat anti–mIL-10 receptor alpha antibody. The plasma concentration-time profiles of mFc–mIL-10 are shown in Fig. 4A, with different doses of the anti–mIL-10 receptor alpha given subcutaneously 1 day before the dosing of mFc–mIL-10. In the absence of the receptor-blocking antibody, the mFc–mIL-10 curve reproduced the i.p. plasma concentration-time profile observed at the same dose in efficacy evaluations. In the presence of the receptor-blocking antibody, the mFc–mIL-10 plasma concentrations did not decline; rather they went up over time in a manner that is consistent with the doses of the receptor-blocking antibody. Figure 4B shows a significant correlation ($P < 0.05$) between the AUC_{tot} of mFc–mIL-10 and the dose of the receptor-blocking antibody. The rising concentrations of mFc–mIL-10 over time are presumably due to the continuous production of the endogenous mIL-10 in the body and the inability of binding to the IL-10 receptor alpha because of the receptor-blocking antibody.

hFc–hIL-10 and hFc–hIL-10 Mutant Pharmacokinetics after Intraperitoneal Administration to Mice. To further provide experimental evidence of the TMDD role in governing the PK of the Fc-fusion proteins, the i.p. PK of an hFc–hIL-10 mutant was studied side by side with the hFc–hIL-10 in mice. As shown in Table 6, the mutant binding affinity to the mIL-10 receptor alpha was 380-fold weaker than that of hFc–hIL-10. Figure 5 shows that hFc–hIL-10 plasma concentrations declined below the LLOQ value ~3 days after i.p. dosing at 0.1 mg/kg, whereas the mutant drug levels given at the same dose were well maintained throughout at least 6 days. The terminal $t_{1/2}$ of hFc–hIL-10 was approximated to be 0.71 ± 0.10 days, significantly different from that (1.9 ± 0.57 days) of the hFc–hIL-10 mutant ($P < 0.05$). One confounding factor to the data interpretation was that the concentrations of hFc–hIL-10 were consistently lower than those of the hFc–hIL-10 mutant by ~4-fold. The data itself may not sufficiently prove the role of TMDD in PK, but it added evidence to other data.

Discussion

Fc fusion is an approach commonly employed to extend the $t_{1/2}$ of peptides, antibody fragments, cytokines, receptor extracellular domains, etc. by increasing the molecular size to reduce the renal filtration and leveraging the FcRn-mediated recycling. Several factors affect the PK of Fc-fusion proteins. These include but are not limited to the degree of glycosylation, binding kinetic differences in the FcRn dissociation between IgG and Fc-fusion proteins, and TMDD (Liu, 2018). In this report, we investigated the PK of Fc–IL-10 fusion proteins and the cause of nonlinear PK observed in mice. Modeling evidence and experimental results were presented to demonstrate the role of TMDD in the PK of Fc–IL-10 fusion proteins at pharmacologically active doses.

Most PK studies presented herein were conducted by the serial sampling of 10 μl blood followed by the dilution of 90 μl Rexxip buffer. To obtain plasma drug concentrations from diluted blood samples, a theoretical dilution factor of 17.36, reported by Joyce et al. (2014), was

TABLE 4

Pharmacokinetic parameters of mIL-10 and hIL-10 after intravenous administration to non–tumor-bearing mice

	mIL-10 (Mean ± S.D., $N = 4$)			hIL-10 (Mean ± S.D., $N = 3$–4)		
	0.05 mg/kg[a]	0.5 mg/kg	5 mg/kg	0.05 mg/kg[a]	0.5 mg/kg	5 mg/kg
C_{max} (nM)[b]	5.3 ± 1.0	218 ± 91	2,161 ± 397	7.0 ± 0.81	141 ± 33	1,513 ± 380
C_{max} ratio[c]	1.0	41	408	1.0	20	216
AUC_{tot} (nM*days)	0.089 ± 0.011	3.7 ± 2.0	34 ± 7.9	0.067 ± 0.002	1.5 ± 0.27	18 ± 2.8
AUC_{tot} ratio[c]	1.0	42	382	1.0	22	269
CL_{tot} (ml/day/kg)	3,836 ± 480	4,341 ± 1732	4,085 ± 941	8,640 ± 208	8,925 ± 1,485	7,557 ± 1,188
V_{ss} (ml/kg)	103 ± 54	139 ± 45	143 ± 38	77 ± 13	193 ± 68	209 ± 112
Terminal $t_{1/2}$ (days)	0.034 ± 0.031	0.067 ± 0.006	0.066 ± 0.016	0.008 ± 0.001[d]	0.045 ± 0.019	0.049 ± 0.010

[a]The dose of 0.05 mg/kg was corrected for drug loss due to nonspecific adsorption in dosing vials and devices. The actual doses used for PK parameter estimations were 0.013 mg/kg for mIL-10 and 0.022 mg/kg for hIL-10. These doses were estimated using compartmental modeling (Table 5; please see text for additional details).
[b]First sampling time point (3 min) after an i.v. bolus dose.
[c]The nominal dose ratio was 1:10:100; the nonspecific adsorption-corrected dose ratios for mIL-10 and hIL-10 were 1:40:400 and 1:23:227, respectively.
[d]Due to the assay sensitivity, the terminal $t_{1/2}$ estimated at the 0.05-mg/kg dose may not represent the terminal phase.

TABLE 5

Compartmental analysis of mFc–mIL-10, mIL-10, hFc–hIL-10, and hIL-10 pharmacokinetic data in tumor-bearing and non–tumor-bearing mice

	mFc–mIL-10 (Mean ± S.D.)	mIL-10 (Mean ± S.D.)	hFc–hIL-10 (Mean ± S.D.)	hIL-10 (Mean ± S.D.)
Intravenous				
V_c (ml/kg)	69 ± 3.5	35 ± 0.23	81 ± 1.9	58 ± 0.65
k_{12} (1/h)	0.213 ± 0.041	1.6 ± 0.034	0.13 ± 0.017	2.6 ± 0.12
k_{21} (1/h)	0.209 ± 0.048	0.88 ± 0.019	0.16 ± 0.023	1.2 ± 0.038
$k_{el,nontarget\text{-}mediated}$ (1/h)	0.019 ± 0.0022	4.3 ± 0.030	0.023 ± 0.00091	5.9 ± 0.097
$K_{m,target\text{-}mediated}$ (nM)	3.2 (fixed)[a]	Not applicable	2.9 (fixed)[a]	Not applicable
$V_{max,target\text{-}mediated}$ (nmol/kg/h)	0.0098 ± 0.0013	Not applicable	0.019 ± 0.0030	Not applicable
% drug remaining in dosing solution at 0.05 mg/kg[b]	38 ± 1.8	25 ± 1.6	52 ± 2.8	44 ± 2.7
Intraperitoneal				
k_a (1/h)	0.25 ± 0.039	Not applicable	Not applicable	Not applicable
$V_{c,apparent}$ (ml/kg)[c]	45 ± 3.0	Not applicable	Not applicable	Not applicable
% drug remaining in dosing solution at 0.03 mg/kg[b]	38 ± 1.8	Not applicable	Not applicable	Not applicable

k_{12}, transfer rate constant from the central to peripheral compartment; k_{21}, transfer rate constant from the peripheral to central compartment.

[a]In vitro IL-10 receptor alpha binding affinity K_d determined by a surface plasmon resonance method.

[b]The drug loss due to nonspecific drug adsorption to dosing vials and devices at the low doses of 0.03–0.05 mg/kg was estimated from fitting the data. The estimations were supported by the in vitro results where the % drug remaining in a dosing solution of 0.02 mg/ml (0.1 mg/kg with a dosing volume of 5 ml/kg) after 2 hours at room temperature was found to be 60%.

[c]$V_{c,apparent}$, as opposed to the i.p. bioavailability, was used as a parameter to model the data after i.p. administration. As described in the text, the i.p. bioavailability after the simultaneous fitting of the mFc–mIL-10 i.v. and i.p. data were estimated to be >100% across a wide dose range (0.03–3 mg/kg), indicating a systematic difference between the i.v. and i.p. studies. Therefore, the $V_{c,apparent}$ was used as a scalar and a more appropriate parameter to fit the i.p. data.

used by assuming that the Fc-fusion proteins and IL-10 did not enter red blood cells and that a hematocrit value was 0.45. The assumptions above were supported by the experimental data generated. First, the serum versus diluted blood concentration ratios of mFc–mIL-10 in matched samples were 13.3 ± 1.9 ($N = 5$). Second, after an i.p. dose of 0.3 mg/kg, the mFc–mIL-10 serum concentration-time profile obtained by composite serum sampling was superimposed to that in plasma after the correction of drug concentrations in diluted blood samples with the theoretical dilution factor (data not shown). Third, the mIL-10 plasma i.v. PK parameters obtained from the diluted blood samples after the correction with the theoretical dilution factor were in agreement with the values reported in the literature (Alvarez et al., 2012). Based on these pieces of evidence, the use of the theoretical dilution factor of 17.36 to obtain plasma drug concentrations from diluted blood samples was justified.

Nonspecific adsorption of cytokines and Fc-fusion proteins to dosing vials and devices sometimes occurs at a low μg/kg dose range. During the compartmental analysis, when the same central compartment volume of distribution (i.e., V_c) was used across the dose range, it was found that the concentration-time profiles predicted from the

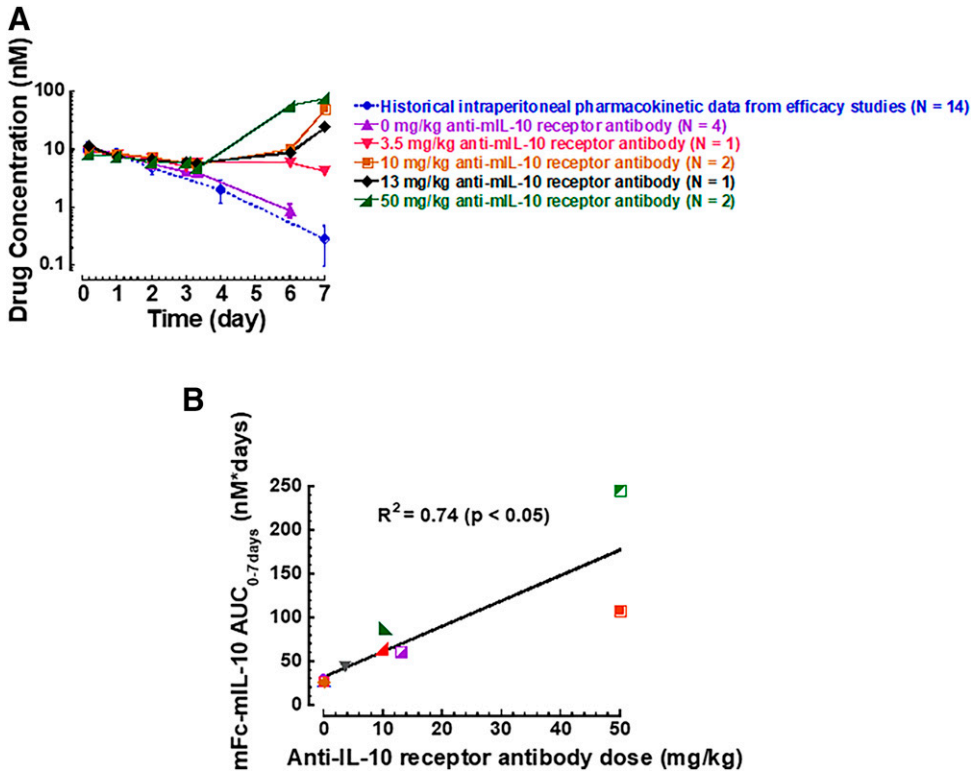

Fig. 4. Target-mediated drug disposition of mFc–mIL-10 was blocked by an anti–mIL-10 receptor alpha antibody. (A) Plasma concentration-time profiles of mFc–mIL-10 after intraperitoneal administration of a 0.1-mg/kg dose to mice in the presence and absence of the anti–mIL-10 receptor alpha antibody; (B) Correlation between the AUC of mFc–mIL-10 and the doses of the anti–mIL-10 receptor alpha antibody in individual mice.

TABLE 6

Pharmacokinetic parameters of hFc–hIL-10 and a mutant of hFc–hIL-10 after intraperitoneal administration of 0.1 mg/kg to non–tumor-bearing mice

	hFc–hIL-10 (Mean ± S.D., N = 4)	hFc–hIL-10 mutant (Mean ± S.D., N = 4)
Binding affinity (nM) to human IL-10 receptor alpha	0.6	2,300
C_{max} (nM)	16 ± 2.8	61 ± 10
T_{max} (h)	9.0 ± 10	4.0 ± 0.0
AUC_{tot} (nM*days)	32 ± 7.9[a]	200 ± 54
Terminal $t_{1/2}$ (days)	0.71 ± 0.10[a]	1.9 ± 0.57

[a]The AUC_{tot} and terminal $t_{1/2}$ shown were approximated values due to an accelerated drug concentration drop at the last measurable time point for hFc–hIL-10.

PK model consistently overpredicted the observed data at the i.v. dose of 0.05 mg/kg and the i.p. dose of 0.03 mg/kg. The overpredictions occurring at the first time point 3 minutes after an i.v. bolus dose cannot be explained by TMDD. As a result, the percentage of drug remaining in the dosing solution as a parameter to account for drug loss due to nonspecific adsorption was introduced to the PK model at the low doses of 0.03–0.05 mg/kg. The approach resulted in a successful data fitting and enabled one set of model parameters to describe the PK data. The need of accounting for nonspecific drug adsorption that led to drug losses in dosing solutions was supported by an in vitro experiment, in which an hFc–hIL-10 solution of 0.02 mg/ml (0.1 mg/kg using 5 ml/kg dosing volume) in a dosing syringe was tested at room temperature for 2 hours and only 60% of the drug concentration was recovered afterward.

In this work, the mFc–mIL-10 and hFc–hIL-10 $t_{1/2}$ (2–4 days) at the doses (e.g., 5 mg/kg) that saturated the TMDD appeared to be shorter than the typical IgG in mice. For example, the IgG1 $t_{1/2}$ in mice was reported to be 6–8 days (Vieira and Rajewsky, 1988). In human FcRn Tg32 homozygous transgenic mice, the average terminal t1/2 from 11 mAbs was ∼10 days (Betts et al., 2018). These findings are consistent with the work done by Unverdorben et al. (2016), in which they found that the terminal $t_{1/2}$ of two Fc-fusion proteins in mice at 1 mg/kg was 4.3–4.6 days versus 9.0–9.3 days for their respective IgG1 antibodies. It is also possible that differences in the glycosylation pattern between IgG and Fc-fusion proteins and inherent instability in Fc-fusion proteins may affect the PK. In our case, PK properties between batches were consistent, suggesting consistent glycosylation patterns in IL-10 Fc-fusion proteins. Additionally, cleavage products in the circulation were examined by liquid chromatography/mass spectrometry (LC/MS) using

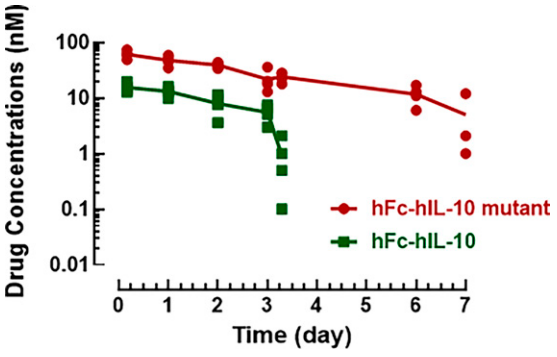

Fig. 5. Plasma concentration-time profiles of hFc–hIL-10 and an hFc–hIL-10 mutant after intraperitoneal administration of a 0.1-mg/kg dose to mice (N = 4 per time point). The line represents the average data in each group. Symbols show individual observed data. When data points are fewer than the number of animals indicated or not shown in the figure, drug concentrations are below the LLOQ (0.08 nM for hFc–hIL-10 and 0.5 nM for the hFc–hIL-10 mutant).

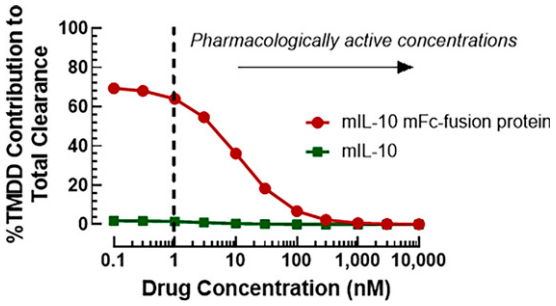

Fig. 6. Contribution of target-mediated drug disposition (TMDD) to the total clearance of mFc–mIL-10 and mIL-10. TMDD was assumed to be the same between the two molecules, and the percentage of the TMDD contribution to the total clearance was calculated based on the parameters presented in Table 5. The dashed line represents the average concentrations of mFc–mIL-10 over 2 to 3 weeks at its pharmacologically active dose of 0.1 mg/kg.

intact mass analysis and a peptide-based approach. No evidence of cleavage products was found (data not shown).

Through the investigation, the cause of nonlinear PK associated with IL-10 Fc-fusion proteins was attributed to TMDD, which led to the terminal $t_{1/2}$ of ∼1 day at pharmacologically active doses in mice. Several pieces of evidence support the conclusion. First, IL-10 receptor alpha is widely expressed in hematopoietic cells. Although the basal expression is 100–700 copies per cell (Tan et al., 1993; von Haehling et al., 2015), the sheer volume of hematopoietic cell counts in the body leads to the IL-10 receptor alpha concentration estimated to be in an nM range. For example, the receptor concentrations in the mouse spleen were estimated to be 0.5–1 nM, based on the total lymphocyte counts of 1.5–2.4 × 10^8 (Berzins et al., 1998; Liu et al., 2005), spleen weight of 0.1 g (Davies and Morris, 1993), and 300 receptor copies per lymphocyte. The target levels were in the same range as the concentrations of IL-10 Fc-fusion proteins at 0.03–0.05 mg/kg, where TMDD had a profound effect on the PK of these molecules. Second, IL-10 is known to bind to glycosaminoglycans, the components of the extracellular matrix in the body, with an affinity of 54 nM (Salek-Ardakani et al., 2000; Künze et al., 2016). However, binding is a distribution process and cannot explain the nonlinear elimination observed with IL-10 Fc-fusion proteins. Additionally, binding to a soluble target may not affect the PK of Fc-fusion proteins as the assays measured the total drug; also, a literature survey did not reveal the presence of high-level targets in the circulation. Third, compartmental analysis unified the nonlinear PK that was observed with IL-10 Fc-fusion proteins, using the Michaelis-Menten kinetics that is commonly employed to describe TMDD. The in vitro binding affinity to the mIL-10 receptor alpha was used successfully as the Michaelis constant $K_{m,target\text{-}mediated}$, suggesting that nonlinear PK is related to the target. Fourth, the studies using a receptor-blocking antibody and a mutant with a reduced target binding affinity demonstrated a meaningful improvement in the terminal $t_{1/2}$ of IL-10 Fc-fusion proteins, providing strong experimental evidence supporting the role of TMDD in the PK of these molecules. Finally, antidrug antibodies for mFc–mIL-10 were detected ≥7 days upon repeat dosing (Supplemental Fig. 5) and cannot explain rapid drug concentration declines within 2 days after dosing at low doses (0.03–0.05 mg/kg).

Compartmental modeling was applied to gain insight into the PK of IL-10 Fc-fusion proteins and IL-10. Dividing the target-mediated clearance ($V_{max,target\text{-}mediated}/K_{m,target\text{-}mediated}$) by the V_c yielded a rate constant ($k_{el,target\text{-}mediated}$) that reflects the target-mediated elimination. Using the values reported in Table 5, the $k_{el,target\text{-}mediated}$ was calculated to be 0.044 $hours^{-1}$ for mFc–mIL-10 and 0.081 $hours^{-1}$ for hFc–hIL-10. These values are ∼2-fold apart, reflecting the comparable binding affinity values to the mIL-10 receptor alpha. When compared with the $k_{el,nontarget\text{-}mediated}$

(0.019–0.023 hours^{-1}) of IL-10 Fc-fusion proteins, the $k_{el,target\text{-}mediated}$ was 2.3- to 3.5-fold higher. These results suggest that when the IL-10 Fc-fusion protein concentrations are below the $K_{m,target\text{-}mediated}$, target-mediated elimination plays a dominant role in governing the PK of these Fc-fusion proteins. In contrast, the $k_{el,nontarget\text{-}mediated}$ estimated for recombinant IL-10 proteins was 4.3–5.9 hours^{-1} (Table 5). When these rate constants were compared with the $k_{el,target\text{-}mediated}$ values mentioned above, the $k_{el,target\text{-}mediated}$ was ~1% of the $k_{el,nontarget\text{-}mediated}$ of recombinant IL-10 proteins. Naturally, the existence of TMDD cannot be detected in the IL-10 PK. Using the PK parameters of mFc–mIL-10 and mIL-10 presented in Table 5, the percentage of the TMDD contribution to the CL_{tot} in a range of concentrations was calculated and is shown in Fig. 6. Between the concentrations of 1 and 10 nM, TMDD contributed to 36%–64% of the CL_{tot} of mFc–mIL-10, whereas its contribution was <2% of the mIL-10 CL_{tot} across the concentration range evaluated. The concentrations of 1 and 10 nM corresponded to the average concentration of mFc–mIL-10 over 2 to 3 weeks at the pharmacologically active dose of 0.1 and 0.3 mg/kg, respectively. At concentrations higher than 10 nM, the TMDD contribution to the mFc–mIL-10 CL_{tot} diminished, indicating that TMDD is saturated. Although TMDD can be saturated at higher drug concentrations or doses, cautions need to be exercised on potential toxicity because the therapeutic index is often narrow for cytokines (Berraondo et al., 2019).

In conclusion, TMDD played an important role in the PK of IL-10 Fc-fusion proteins at pharmacologically active doses. Compartmental modeling results and experimental evidence generated with a receptor-block antibody and a mutant strongly supported the conclusion. Future drug design with Fc-fusion proteins needs to consider target expression and examine its effect on PK. When conducting PK studies, a dose range covering pharmacological activity is crucial.

Authorship Contributions

Participated in research design: Yang, Rajendran, Poirson, Gururajan, Loy, Vasudevan, Broz, Lehman-McKeeman, Morin, Graziano.

Conducted experiments: Rajendran, Spires, Poirson, Arbanas, Cheng, Carl, Pace, Wang, Mehl, Xu.

Contributed new reagents or analytic tools: Lin, Krystek, Morin.

Performed data analysis: Yang, Spires, Poirson, Arbanas.

Wrote or contributed to the writing of the manuscript: Yang, Rajendran, Spires, Poirson, Arbanas, Broz, Lehman-McKeeman, Morin, Graziano.

References

Abdiche YN, Yeung YA, Chaparro-Riggers J, Barman I, Strop P, Chin SM, Pham A, Bolton G, McDonough D, Lindquist K, et al. (2015) The neonatal Fc receptor (FcRn) binds independently to both sites of the IgG homodimer with identical affinity. *MAbs* **7**:331–343.

Adris S, Klein S, Jasnis M, Chuluyan E, Ledda M, Bravo A, Carbone C, Chernajovsky Y, and Podhajcer O (1999) IL-10 expression by CT26 colon carcinoma cells inhibits their malignant phenotype and induces a T cell-mediated tumor rejection in the context of a systemic Th2 response. *Gene Ther* **6**:1705–1712.

Alvarez HM, So OY, Hsieh S, Shinsky-Bjorde N, Ma H, Song Y, Pang Y, Marian M, and Escandón E (2012) Effects of PEGylation and immune complex formation on the pharmacokinetics and biodistribution of recombinant interleukin 10 in mice. *Drug Metab Dispos* **40**:360–373.

An G (2020) Concept of pharmacologic target-mediated drug disposition in large-molecule and small-molecule compounds. *J Clin Pharmacol* **60**:149–163.

Berman RM, Suzuki T, Tahara H, Robbins PD, Narula SK, and Lotze MT (1996) Systemic administration of cellular IL-10 induces an effective, specific, and long-lived immune response against established tumors in mice. *J Immunol* **157**:231–238.

Berraondo P, Sanmamed MF, Ochoa MC, Etxeberria I, Aznar MA, Pérez-Gracia JL, Rodríguez-Ruiz ME, Ponz-Sarvise M, Castañón E, and Melero I (2019) Cytokines in clinical cancer immunotherapy. *Br J Cancer* **120**:6–15.

Berzins SP, Boyd RL, and Miller JF (1998) The role of the thymus and recent thymic migrants in the maintenance of the adult peripheral lymphocyte pool. *J Exp Med* **187**:1839–1848.

Betts A, Keunecke A, van Steeg TJ, van der Graaf PH, Avery LB, Jones H, and Berkhout J (2018) Linear pharmacokinetic parameters for monoclonal antibodies are similar within a species and across different pharmacological targets: a comparison between human, cynomolgus monkey and hFcRn Tg32 transgenic mouse using a population-modeling approach. *MAbs* **10**:751–764.

Davies B and Morris T (1993) Physiological parameters in laboratory animals and humans. *Pharm Res* **10**:1093–1095.

Emmerich J, Mumm JB, Chan IH, LaFace D, Truong H, McClanahan T, Gorman DM, and Oft M (2012) IL-10 directly activates and expands tumor-resident CD8(+) T cells without de novo infiltration from secondary lymphoid organs. *Cancer Res* **72**:3570–3581.

Hecht JR, Lonardi S, Bendell J, Sim HW, Macarulla T, Lopez CD, Van Cutsem E, Muñoz Martin AJ, Park JO, Greil R, et al. (2021) Randomized phase III study of FOLFOX alone or with pegilodecakin as second-line therapy in patients with metastatic pancreatic cancer that progressed after gemcitabine (SEQUOIA). *J Clin Oncol* **39**:1108–1118.

Huhn RD, Radwanski E, O'Connell SM, Sturgill MG, Clarke L, Cody RP, Affrime MB, and Cutler DL (1996) Pharmacokinetics and immunomodulatory properties of intravenously administered recombinant human interleukin-10 in healthy volunteers. *Blood* **87**:699–705.

Joyce AP, Wang M, Lawrence-Henderson R, Filliettaz C, Leung SS, Xu X, and O'Hara DM (2014) One mouse, one pharmacokinetic profile: quantitative whole blood serial sampling for biotherapeutics. *Pharm Res* **31**:1823–1833.

Jung K, Ha JH, Kim JE, Kim JA, Kim YJ, Kim CH, and Kim YS (2018) Heterodimeric Fc-fused IL12 shows potent antitumor activity by generating memory CD8$^+$ T cells. *OncoImmunology* **7**:e1438800.

Kontermann RE (2016) Half-life extended biotherapeutics. *Expert Opin Biol Ther* **16**:903–915.

Kuna M, Mahdi F, Chade AR, and Bidwell 3rd GL (2018) Molecular size modulates pharmacokinetics, biodistribution, and renal deposition of the drug delivery biopolymer elastin-like polypeptide. *Sci Rep* **8**:7923.

Künze G, Köhling S, Vogel A, Rademann J, and Huster D (2016) Identification of the glycosaminoglycan binding site of interleukin-10 by NMR spectroscopy. *J Biol Chem* **291**:3100–3113.

Liu JY, Zhang XS, Ding Y, Peng RQ, Cheng X, Zhang NH, Xia JC, and Zeng YX (2005) The changes of CD4+CD25+/CD4+ proportion in spleen of tumor-bearing BALB/c mice. *J Transl Med* **3**:5.

Liu L (2018) Pharmacokinetics of monoclonal antibodies and Fc-fusion proteins. *Protein Cell* **9**:15–32.

Liu Y, Wei SH, Ho AS, de Waal Malefyt R, and Moore KW (1994) Expression cloning and characterization of a human IL-10 receptor. *J Immunol* **152**:1821–1829.

Moore KW, de Waal Malefyt R, Coffman RL, and O'Garra A (2001) Interleukin-10 and the interleukin-10 receptor. *Annu Rev Immunol* **19**:683–765.

Mumm JB, Emmerich J, Zhang X, Chan I, Wu L, Mauze S, Blaisdell S, Basham B, Dai J, Grein J, et al. (2011) IL-10 elicits IFNγ-dependent tumor immune surveillance. *Cancer Cell* **20**:781–796.

Naing A, Infante JR, Papadopoulos KP, Chan IH, Shen C, Ratti NP, Rojo B, Autio KA, Wong DJ, Patel MR, et al. (2018) PEGylated IL-10 (pegilodecakin) induces systemic immune activation, CD8$^+$ T cell invigoration and polyclonal T cell expansion in cancer patients. *Cancer Cell* **34**:775–791.e3.

Ray AL, Nofchissey RA, Khan MA, Reidy MA, Lerner MR, Wu X, Guo S, Hill SL, Weygant N, Adams SF, et al. (2020) The role of sex in the innate and adaptive immune environment of metastatic colorectal cancer. *Br J Cancer* **123**:624–632.

Rhode PR, Egan JO, Xu W, Hong H, Webb GM, Chen X, Liu B, Zhu X, Wen J, You L, et al. (2016) Comparison of the superagonist complex, ALT-803, to IL15 as cancer immunotherapeutics in animal models. *Cancer Immunol Res* **4**:49–60.

Runbeck E, Crescioli S, Karagiannis SN, and Papa S (2021) Utilizing immunocytokines for cancer therapy. *Antibodies (Basel)* **10**:10.

Salek-Ardakani S, Arrand JR, Shaw D, and Mackett M (2000) Heparin and heparan sulfate bind interleukin-10 and modulate its activity. *Blood* **96**:1879–1888.

Shouval DS, Ouahed J, Biswas A, Goettel JA, Horwitz BH, Klein C, Muise AM, and Snapper SB (2014) Interleukin 10 receptor signaling: master regulator of intestinal mucosal homeostasis in mice and humans. *Adv Immunol* **122**:177–210.

Tan JC, Indelicato SR, Narula SK, Zavodny PJ, and Chou C-C (1993) Characterization of interleukin-10 receptors on human and mouse cells. *J Biol Chem* **268**:21053–21059.

Tannir NM, Papadopoulos KP, Wong DJ, Aljumaily R, Hung A, Afable M, Kim JS, Ferry D, Drakaki A, Bendell J, et al. (2021) Pegilodecakin as monotherapy or in combination with anti-PD-1 or tyrosine kinase inhibitor in heavily pretreated patients with advanced renal cell carcinoma: final results of cohorts A, G, H and I of IVY phase I study. *Int J Cancer* **149**:403–408.

Unverdorben F, Richter F, Hutt M, Seifert O, Malinge P, Fischer N, and Kontermann RE (2016) Pharmacokinetic properties of IgG and various Fc fusion proteins in mice. *MAbs* **8**:120–128.

Vazquez-Lombardi R, Loetsch C, Zinkl D, Jackson J, Schofield P, Deenick EK, King C, Phan TG, Webster KE, Sprent J, et al. (2017) Potent antitumour activity of interleukin-2-Fc fusion proteins requires Fc-mediated depletion of regulatory T-cells. *Nat Commun* **8**:15373.

Vieira P and Rajewsky K (1988) The half-lives of serum immunoglobulins in adult mice. *Eur J Immunol* **18**:313–316.

von Haehling S, Wolk K, Höflich C, Kunz S, Grünberg BH, Döcke WD, Reineke U, Asadullah K, Sterry W, Volk HD, et al. (2015) Interleukin-10 receptor-1 expression in monocyte-derived antigen-presenting cell populations: dendritic cells partially escape from IL-10's inhibitory mechanisms [published correction appears in Genes Immun (2015) 16:366]. *Genes Immun* **16**:8–14.

Walter MR (2014) The molecular basis of IL-10 function: from receptor structure to the onset of signaling. *Curr Top Microbiol Immunol* **380**:191–212.

Wang F, Tsai JC, Davis JH, Chau B, Dong J, West SM, Hogan JM, Wheeler ML, Bee C, Morishige W, et al. (2020) Design and characterization of mouse IgG1 and IgG2a bispecific antibodies for use in syngeneic models. *MAbs* **12**:1685350.

Zhang Y, Huo M, Zhou J, and Xie S (2010) PKSolver: an add-in program for pharmacokinetic and pharmacodynamic data analysis in Microsoft Excel. *Comput Methods Programs Biomed* **99**:306–314.

Zhu EF, Gai SA, Opel CF, Kwan BH, Surana R, Mihm MC, Kauke MJ, Moynihan KD, Angelini A, Williams RT, et al. (2015) Synergistic innate and adaptive immune response to combination immunotherapy with anti-tumor antigen antibodies and extended serum half-life IL-2. *Cancer Cell* **27**:489–501.

Address correspondence to: Zheng Yang, Bristol Myers Squibb, Route 206 and Province Line Road, Princeton, NJ 08543-4000. E-mail: yangz@bms.com

Drug Metabolism and Disposition: DMD-AR-2021-000799

Target-Mediated Drug Disposition Affects the Pharmacokinetics of Interleukin-10 Fc-fusion Proteins at Pharmacologically Active Doses

Authors: Zheng Yang, Surendran Rajendran, Vanessa Spires, Brian Poirson, Murali Gururajan, Zheng Lin, Jaren Arbanas, Stanley Krystek, James Loy, Yuan Cheng, Stephen Carl, Samantha Pace, Yun Wang, John Mehl, Shihua Xu, Krishna Vasudevan, Miranda Broz, Lois Lehman-McKeeman, Paul Morin, and Robert F. Graziano

Affiliation: Bristol Myers Squibb Company, Princeton, New Jersey, U.S.A.

SUPPLEMENTAL MATERIALS AND REAGENTS

1. Structural Sequences of IL-10 and IL-10 Fc-fusion Proteins

mIL-10

```
1    SRGQY SREDN NCTHF PVGQS HMLLE LRTAF SQVKT FFQTK
41   DQLDN ILLTD SLMQD FKGYL GCQAL SEMIQ FYLVE VMPQA
81   EKHGP EIKEH LNSLG EKLKT LRMRL RRCHR FLPCE NKSKA
121  VEQVK SDFNK LQDQG VYKAM NEFDI FINCI EAYMM IKMKS
```

hIL-10

```
1    SRGQG TQSEN SCTHF PGNLP NMLRD LRDAF SRVKT FFQMK
41   DQLDN LLLKE SLLED FKGYL GCQAL SEMIQ FYLEE VMPQA
81   ENQDP DIKAH VNSLG ENLKT LRLRL RRCHR FLPCE NKSKA
121  VEQVK NAFNK LQEKG IYKAM SEFDI FINYI EAYMT MKIRN
```

mFc-mIL-10

```
1    VPRDCGCKPC ICTVPEVSSV FIFPPKPKDV LTITLTPKVT CVVVAISKDD
51   PEVQFSWFVD DVEVHTAQTQ PREEQFNSTF RSVSELPIMH QDWLNGKEFK
101  CRVNSAAFPA PIEKTISKTK GRPKAPQVYT IPPPKEQMAK DKVSLTCMIT
151  DFFPEDITVE WQWNGQPAEN YKNTQPIMDT DGSYFVYSKL NVQKSNWEAG
201  NTFTCSVLHE GLHNHHTEKS LSHSPGGGGG SGGGGSGGGG SGGGGSSRGQ
251  YSREDNNCTH FPVGQSHMLL ELRTAFSQVK TFFQTKDQLD NILLTDSLMQ
301  DFKGYLGCQA LSEMIQFYLV EVMPQAEKHG PEIKEHLNSL GEKLKTLRMR
351  LRRCHRFLPC ENKSKAVEQV KSDFNKLQDQ GVYKAMNEFD IFINCIEAYM
401  MIKMKS
```

hFc-hIL-10

```
1     DKTHTCPPCP APEAEGAPSV FLFPPKPKDT LMISRTPEVT CVVVDVSHED
51    PEVKFNWYVD GVEVHNAKTK PREEQYNSTY RVVSVLTVLH QDWLNGKEYK
101   CKVSNKALPA PIEKTISKAK GQPREPQVYT LPPSREEMTK NQVSLTCLVK
151   GFYPSDIAVE WESNGQPENN YKTTPPVLDS DGSFFLYSKL TVDKSRWQQG
201   NVFSCSVMHE ALHNHYTQKS LSLSPGGGGG SSGGGGSGGG GSGGGGSSPG
251   QGTQSENSCT HFPGNLPNML RDLRDAFSRV KTFFQMKDQL DNLLLKESLL
301   EDFKGYLGCQ ALSEMIQFYL EEVMPQAENQ DPDIKAHVNS LGENLKTLRL
351   RLRRCHRFLP CENKSKAVEQ VKNAFNKLQE KGIYKAMSEF DIFINYIEAY
401   MTMKIRN
```

hFc-hIL-10 mutant

```
1     DKTHTCPPCP APEAEGAPSV FLFPPKPKDT LMISRTPEVT CVVVDVSHED
51    PEVKFNWYVD GVEVHNAKTK PREEQYNSTY RVVSVLTVLH QDWLNGKEYK
101   CKVSNKALPA PIEKTISKAK GQPREPQVYT LPPSREEMTK NQVSLTCLVK
151   GFYPSDIAVE WESNGQPENN YKTTPPVLDS DGSFFLYSKL TVDKSRWQQG
201   NVFSCSVMHE ALHNHYTQKS LSLSPGGGGG SSGGGGSGGG GSGGGGSSPG
251   QGTQSENSCT HFPGNLPNML SDLRDAFSRV KTFFSMKDQL DNSLLKESLL
301   EDFKGYLGCQ ALSEMIQFYL EEVMPQAENQ DPDIKAHVNS LGENLKTLRL
351   RLRRCHRFLP CENKSKAVEQ VKNAFNKLQE KGIYKAMSEF DIFINYIEAY
401   MTMKIRN
```

2. Characterizations of IL-10 and IL-10 Fc-fusion Proteins

	mIL-10	hIL-10	mFc-mIL-10	hFc-hIL-10	hFc-hIL-10 Mutant
Molecular Weight (Da)*	18,751	18,703	91,004	90,815	90,542
Aggregation status					
High molecular weight aggregates	<5%	<5%	<5%	<5%	<5%
Low molecular weight components	<5%	<5%	<5%	<5%	<5%
Endotoxin (EU/mL)	<0.075	<0.075	<0.075	<0.075	<0.075

*Theoretical mass of deglycosylated form.

Primary structures of all five protein analytes (mIL-10, hIL-10, mFc-mIL-10, hFc-hIL10, and hFc-hIL-10 mutant) used in this publication were confirmed by LC/MS/MS peptide mapping with >97% sequence coverage. The molecular weights of the intact versions of these proteins verified by LC/MS were consistent with the theoretical masses calculated from the respective protein amino acid sequences.

SUPPLEMENTAL TABLE

Supplemental Table 1. Key Models Tested and Fitting Performance for mFc-mIL-10 Pharmacokinetic Data after Intravenous and Intraperitoneal Administration to Tumor- and Non-tumor-bearing Mice

Model	Objective function[a,b]	Akaike information criterion[b]	Schwarz-Bayesian information criterion[b]
1-compartment model with target- and non-target-mediated elimination	839	869	897
2-compartment model with target-mediated elimination only	839	870	900
2-compartment model with target- and non-target-mediated elimination (**final model**)	812	842	874

a. Expressed as -2 times the log-likelihood function.
b. Converted from the output statistics in SAAM II.

Supplemental Table 2. Key Models Tested and Fitting Performance for hFc-hIL-10 Pharmacokinetic Data after Intravenous Administration to Non-tumor-bearing Mice

Model	Objective function[a,b]	Akaike information criterion[b]	Schwarz-Bayesian information criterion[b]
1-compartment model with target- and non-target-mediated elimination	409	424	432
2-compartment model with target-mediated elimination only	407	422	432
2-compartment model with target- and non-target-mediated elimination (**final model**)	357	375	387

a. Expressed as -2 times the log-likelihood function.
b. Converted from the output statistics in SAAM II.

Supplemental Table 3. Key Models Tested and Fitting Performance for mIL-10 Pharmacokinetic Data after Intravenous Administration to Non-tumor-bearing Mice

Model	Objective function[a,b]	Akaike information criterion[b]	Schwarz-Bayesian information criterion[b]
1-compartment model with non-target-mediated elimination only	4,335	4,320	4,320
2-compartment model with target- and non-target-mediated elimination[c]	404	414	421
2-compartment model with non-target-mediated elimination only (**final model**)	407	418	421

a. Expressed as -2 times the log-likelihood function.
b. Converted from the output statistics in SAAM II.
c. The target binding affinity of mIL-10 was assumed to be the same as that (3.2 nM) of mFc-mIL-10 in mice.

Supplemental Table 4. Key Models Tested and Fitting Performance for hIL-10 Pharmacokinetic Data after Intravenous Administration to Non-tumor-bearing Mice

Model	Objective function[a,b]	Akaike information criterion[b]	Schwarz-Bayesian information criterion[b]
1-compartment model with non-target-mediated elimination only	2,490	2,492	2,492
2-compartment model with target- and non-target-mediated elimination[c]	261	273	277
2-compartment model with non-target-mediated elimination only (**final model**)	280	290	294

a. Expressed as -2 times the log-likelihood function.

b. Converted from the output statistics in SAAM II.

c. The target binding affinity of hIL-10 was assumed to be the same as that (2.9 nM) of hFc-hIL-10 in mice.

SUPPLEMENTAL FIGURE

Supplemental Figure 1. Diagnostic Plots Obtained from Pharmacokinetic Modeling of mFc-mIL-10 Average Concentration Data after Intravenous and Intraperitoneal Administration to Tumor- and Non-tumor-bearing Mice

a. Predicted vs. observed concentrations

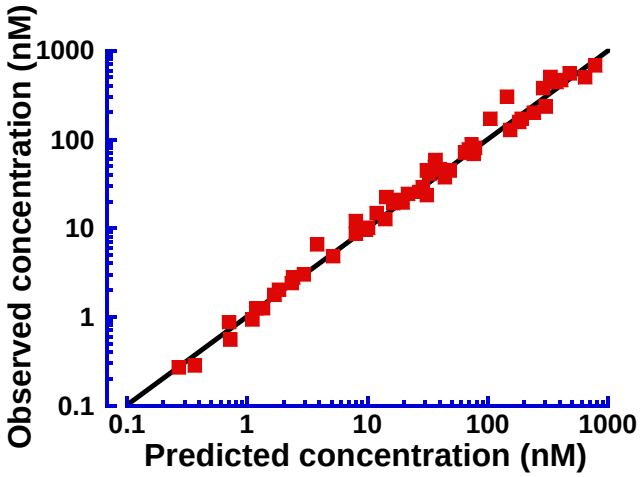

b. Weighted residuals vs. predicted concentrations

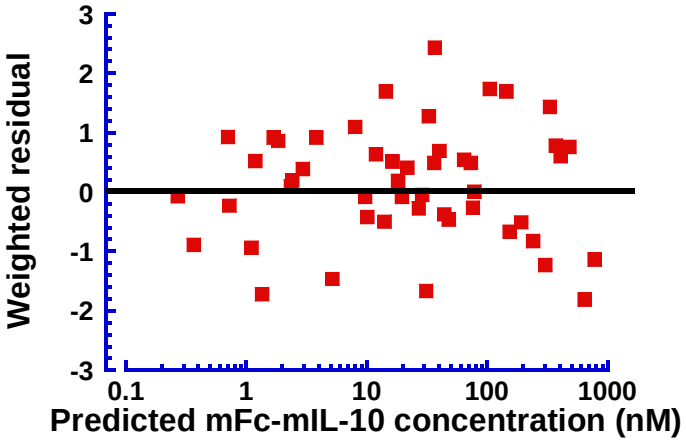

Supplemental Figure 2. Diagnostic Plots Obtained from Pharmacokinetic Modeling of hFc-hIL-10 Average Concentration Data after Intravenous Administration to Non-tumor-bearing Mice

a. Predicted vs. observed concentrations

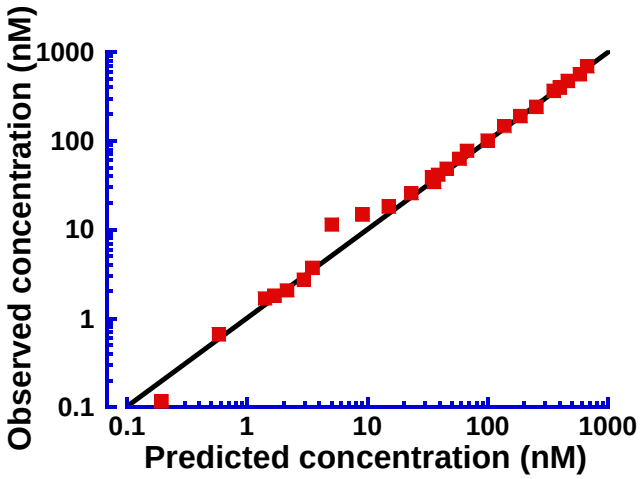

b. Weighted residuals vs. predicted concentrations

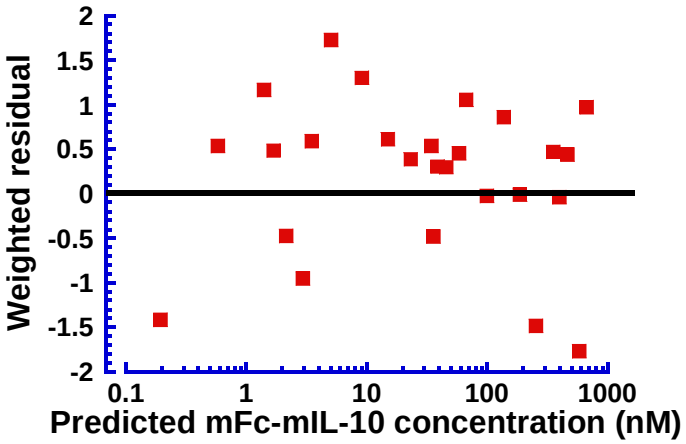

Supplemental Figure 3. Diagnostic Plots Obtained from Pharmacokinetic Modeling of mIL-10 Average Concentration Data after Intravenous Administration to Non-tumor-bearing Mice

a. Predicted vs. observed concentrations

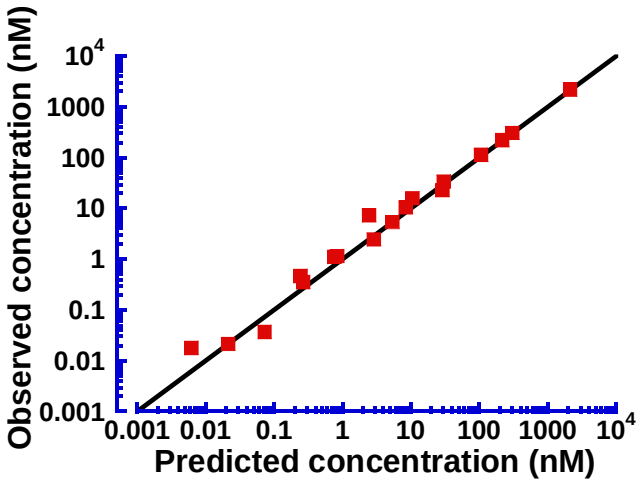

b. Weighted residuals vs. predicted concentrations

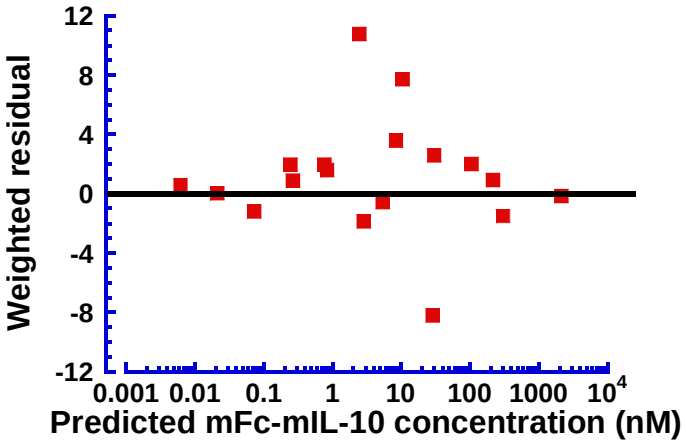

Supplemental Figure 4. Diagnostic Plots Obtained from Pharmacokinetic Modeling of hIL-10 Average Concentration Data after Intravenous Administration to Non-tumor-bearing Mice

a. Predicted vs. observed concentrations

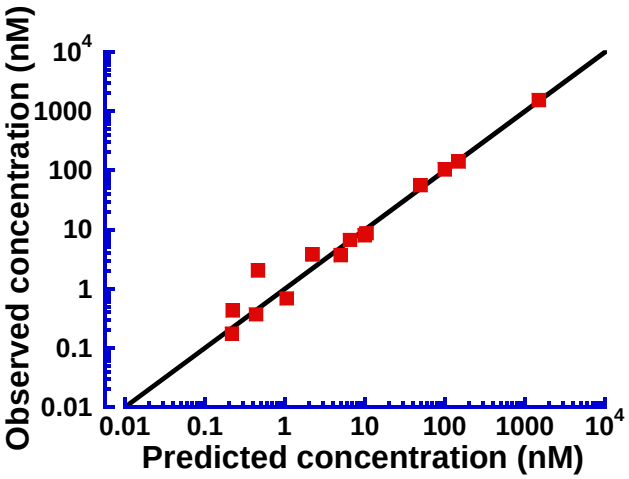

b. Weighted residuals vs. predicted concentrations

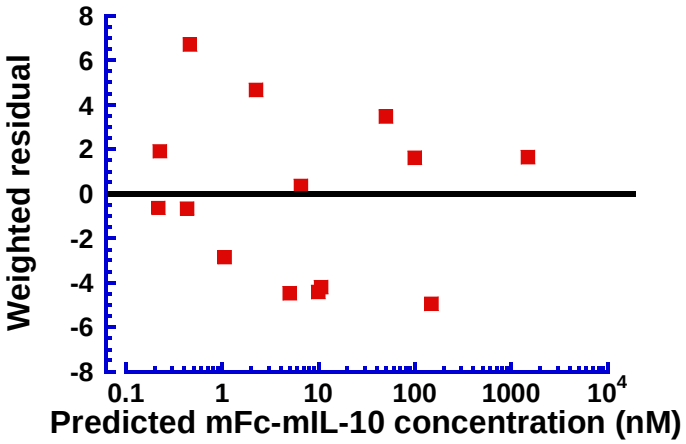

Supplemental Figure 5. **Time Course of Anti-mFc-mIL-10 Antibody Titers in the Mouse CT26 Syngeneic Tumor Model following Intraperitoneal Administration of mFc-mIL-10 and a Mouse Anti-mPD-1 Monoclonal Antibody**

(Note: mFc-mIL-10 was dosed weekly (QW) for 3 doses and the mouse anti-mPD-1 monoclonal antibody was given every 4 days (Q4D) for 6 doses. Anti-mFc-mIL-10 antibodies in mouse serum samples were detected by a ligand-binding assay on a chemiluminescence platform developed at Bristol Myers Squibb, with mFc-mIL-10 and peroxidase AffiniPure rat anti-mouse IgG (H+L) (Jackson ImmunoResearch Laboratories Inc., West Grove, PA) used as the capture and detection reagents, respectively. The line represents the average value of the data.)